

Facile Synthesis of Transition Metals (Co-Ni) Gallates and their Electrochemical Applications



By

Aqsa Shabbir

(Registration No: 00000403000)

This thesis is submitted to the National University of Sciences and Technology, Islamabad,

in partial fulfillment of the requirements for the degree of

Master of Science in
Chemistry

Supervisor: Dr. Manzar Sohail

School of Natural Sciences

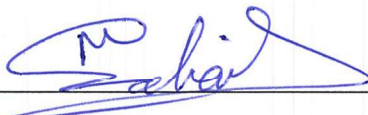
National University of Sciences & Technology (NUST)

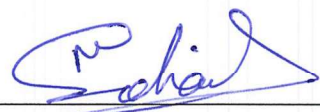
Islamabad, Pakistan


(2024)

THESIS ACCEPTANCE CERTIFICATE

Certified that final copy of MS thesis written by Aqsa Shabbir (Registration No. 00000403000), of School of Natural Sciences has been vetted by undersigned, found complete in all respects as per NUST statutes/regulations, is free of plagiarism, errors, and mistakes and is accepted as partial fulfillment for award of MS/M.Phil degree. It is further certified that necessary amendments as pointed out by GEC members and external examiner of the scholar have also been incorporated in the said thesis.

Signature: 
Name of Supervisor: Prof. Manzar Sohail
Date: 09/01/2025

Signature (HoD): 
Date: 09/01/2025

Signature (Dean/Principal): 
Date: 10.01.2025

National University of Sciences & Technology

MS THESIS WORK

We hereby recommend that the dissertation prepared under our supervision by: Aqsa Shabbir, Regn No. 00000403000 Titled Facile Synthesis of Transition Metals (Co-Ni) Gallates and Their Electrochemical Application be Accepted in partial fulfillment of the requirements for the award of MS degree.

Examination Committee Members

1. Name: DR. GHULAM HUSSAIN

Signature: 

2. Name: DR. INAYAT ALI KHAN

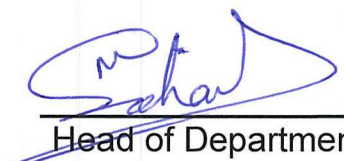
Signature: 

3. Name: DR. MUHAMMAD KASHIF MAJEED

Signature: 

Supervisor's Name PROF. MANZAR SOHAIL

Signature: 


Head of Department

09/01/2025
Date

COUNTERSIGNED

Date: 10.01.2025


Dean/Principal

DEDICATION

“To the tenacious Palestinian people,

You are the resilient olive trees that have been planted in the soil of your native region for generations, bearing testimony to hardship and hope. This work is dedicated to you. You are the rivers that flow through the valleys of history with hopes of freedom, and you are the unwavering mountains that stand tall against the winds of adversity.

In the darkest of nights, your bravery is like a lantern's light—a glimmer of hope for justice that never goes out. As they say, "The scar tells the story, even though the wound may heal"

Your wounds bear witness to your tenacity, fortitude, and unshakeable faith in the face of injustice.

May your spirit be honored and your voices heard, reminding the world that even the tiniest grain of sand may transform into a pearl of great value when put under strain. This piece honors your undying desire to bloom even in the most hostile deserts and is simply a drop in the ocean of your tenacity.

This is for your unwavering hope and the endless horizon of peace you work towards, to you who never stop inspiring”

ACKNOWLEDGEMENTS

Starting with the name of Allah Almighty, I am deeply thankful to Allah Almighty for giving me the courage, patience, and wisdom to accomplish my thesis. Without His blessings, this accomplishment would not have been achievable.

I am extremely thankful to my supervisor who has put in to ensure the success of this endeavor, as well as for consistently inspiring me to strive for perfection. Their mentoring has had a significant impact on my personal and professional development, in addition to improving my academic performance. Thank you for your ongoing drive and belief in my abilities. I am also thankful to my GEC members, **Dr. Muhammad Kashif Majeed, Dr. Inayat Ali Khan, and Dr. Ghulam Hussain** for their insightful comments and helpful criticism, which have substantially improved my work. Your inspiration and assistance have been crucial to my development and education.

With all my heart, I dedicate this work to **my dear parents**, and my Taya Abu **Muhammad Yaseen**, whose unshakeable love, sacrifices, and prayers have been the foundation for every success in my life. I owe everything to my mother for her limitless love, gentle wisdom, and unwavering belief in my dreams; and to my father for his leadership, tenacity, and the innumerable lessons that have shaped me into who I am today. Your unselfish efforts and innumerable sacrifices have illuminated my path and encouraged me to achieve heights

To my closest friends, **Sobia Rafique, Faiza Yasir, Hadia Naqash, and Nimra Shabbir** I have found comfort in your unwavering support, humor, and encouragement throughout trying times. You have encouraged me to never give up hope and to enjoy the journey. I want to thank my seniors especially **Saddam Hussain, Maria Masood, Aashir Awan, Ifra Urooj** and my fellows of lab 110, **Muhammad Ahmed, Ayesha Arif, Aamal Rehman, and Umer Farooq** for making the lab feel like a family. Even the most challenging jobs were transformed into unforgettable experiences by your cooperation, guidance, and friendship.

God! I have so many people to be grateful to. You have all been invaluable to my path, and I will always be appreciative of your generosity and constant support. This accomplishment is both yours and mine.

Aqsa Shabbir

ABSTRACT

This work created several catalysts using a solventless technique, removing the requirement for hazardous solvents. This highlights sustainability and green chemistry concepts. With an emphasis on their use in the oxygen evolution process (OER), the produced catalysts were methodically characterized to investigate their structural, morphological, and electrochemical characteristics. Electrochemical analysis determined the catalysts' exceptional OER activity. The top-performing catalyst at a current density of 50 mA/cm^2 , displayed an exceptionally low overpotential of 300 mV, highlighting its great catalytic efficiency. A result of 96.42 mV/dec from the Tafel slope analysis indicated good reaction kinetics and effective charge transfer at the electrode contact. The catalysts' large electrochemical active surface area of the catalysts was validated by capacitance measurements resulting from electrochemical double-layer capacitance. The greatest C_{dl} value, which reached 27.5 mF/cm^2 , indicated an excess of active sites for the OER process. The catalysts' exceptional performance was further verified by electrochemical impedance spectroscopy, which showed that the best-performing sample had a charge transfer resistance of just 23Ω , indicating quick electron transfer during the catalytic process. This study emphasizes the solventless synthesis process as a successful and sustainable strategy for creating high-performance OER catalysts. The results offer insightful information on the connection between structural characteristics and electrochemical performance, opening the door for further advancements in sustainable energy technology.

Table of Contents

DEDICATION	i
ACKNOWLEDGEMENTS.....	ii
ABSTRACT.....	iii
List of abbreviations	ix
Chapter 1: Introduction.....	1
1.1. Energy Crisis.....	1
1.2. Challenges.....	4
1.3. Hydrogen as a promising solution	4
1.4. Sources of hydrogen production	5
1.5. Future Trends and Innovations.....	7
1.6. Water splitting.....	8
1.6.1. Thermodynamics of Water Splitting	8
1.6.2. Chemical Pathway	8
1.6.3. Mechanistic insights.....	9
1.6.4. Factors affecting Water Splitting:	9
1.7. Types of water splitting:.....	9
1.7.1. Photocatalytic water splitting.....	10
1.7.2. Photoelectrochemical water splitting.....	12
1.7.3. Photovoltaic-integrated photoelectrochemical (PEC) water splitting.....	12
1.7.4. Introduction to Electrochemical water splitting:.....	13
1.8. Mechanism of Oxygen Evolution Reaction.....	13
1.9. Mechanism of Hydrogen Evolution Reaction.....	14
1.10. Fundamental Electrochemistry of Water Splitting.....	15
1.11. Electrochemistry involved in EWS.....	18
1.12. Spinel structures as electrocatalyst for WS.....	19
1.12.1. Structure of Spinel.....	19

1.12.2.	Examples of Spinels.....	20
1.12.3.	Properties of Spinels	20
1.12.4.	Applications for Spinels.....	20
1.13.	CoGa ₂ O ₄ as an electrocatalyst	21
1.13.2.	Advantages of using NiGa ₂ O ₄	22
Chapter 2: Literature Review.....		23
Chapter 3: Experimentation		27
3.1.	Materials	27
3.2.	Apparatus and Glassware.....	27
3.3.	Synthesis of CoGa ₂ O ₄	27
3.4.	Synthesis of NiGa ₂ O ₄	28
3.5.	Synthesis of Co _x Ni _{1-x} Ga ₂ O ₄	28
3.6.	Fabrication of electrode:	29
Chapter 4: Results and Discussion.....		31
4.1.	X-ray Diffraction Analysis.....	31
4.1.1.	XRD Analysis	31
4.1.1.1.	Interpretation of Specific Samples.....	32
4.2.	Fourier Transform Infrared Spectroscopy.....	32
4.2.1.	FTIR Analysis	33
4.2.1.1.	Key Observations.....	34
4.3.	Scanning electron Microscopy.....	34
4.3.1.	SEM Analysis.....	35
4.3.1.1.	Key Observations.....	35
4.4.	Energy Dispersive Spectroscopy	36
4.4.1.	EDS Analysis	37
4.5.	Transmission Electron Microscopy	38
4.5.1.	TEM Analysis	38

4.5.1.1. Key Observations.....	38
4.6. Differential Scanning Calorimetry.....	39
4.6.1. DSC analysis.....	39
4.6.1. Key Observations.....	39
4.7. Electrochemical Analysis.....	40
4.8. Oxygen Evolution Reaction.....	42
4.8.1. Electrochemically Active Surface Area	45
4.8.2. Electron Impedance Spectroscopy.....	47
Chapter 5: Conclusion.....	50
References.....	52

Table of Figures

Figure 1. Energy supply from 1990 to 2020. a) Energy supply and b) Energy consumption. EJ: extra joules.[6]	3
Figure 2. Schematic diagram for the synthesis of CoGa_2O_4	27
Figure 3. Schematic diagram for the synthesis of NiGa_2O_4	28
Figure 4. Schematic diagram for the synthesis of $\text{Co}_x\text{Ni}_{1-x}\text{Ga}_2\text{O}_4$	29
Figure 5. Schematic diagram for the fabrication of electrodes	30
Figure 6. XRD spectra of CG, CNG-1, CNG-2, CNG-3, CNG-4, CNG-5, and NG	31
Figure 7. FTIR spectra of CG, CNG-1, CNG-2, CNG-3, CNG-4, CNG-5, and NG	33
Figure 8. Scanning electron microscopy (SEM) images of a) CG, b) CNG-1, c) CNG-2, d) CNG-3, e) CNG-4, f) CNG-5, and g) NG at a resolution of $5\mu\text{m}$	35
Figure 9. EDX spectra of a) CG, b) CNG-1, c) CNG-2, d) CNG-3, e) CNG-4, f) CNG-5, and g) NG.	37
Figure 10. Transmission Electron Microscopy images of CNG-5 at a) 1nm, b) 2nm, c) 5nm with an inset showing IFFT image, and d) live profile image showing interplanar d spacing.	38
Figure 11. DSC analysis of CNG-4.....	40
Figure 12. a) Linear Sweep Voltammetry (LSV) curves, and b) bar graph showing overpotential values of CG, CNG-1, CNG-2, CNG-3, CNG-4, CNG-5, and NG at 50 mA with a scan rate of 5 mV s^{-1} in 1 M KOH	43
Figure 13. Tafel slope values of CG, CNG-1, CNG-2, CNG-3, CNG-4, CNG-5, and NG at current density of 50 mA.	44
Figure 14. C_{dl} values of CG, CNG-1, CNG-2, CNG-3, CNG-4, CNG-5, and NG	46
Figure 15. a) Nyquist plots, and b) bar graph showing R_{ct} values of CG, CNG-1, CNG-2, CNG-3, CNG-4, CNG-5, and NG.....	49

List of tables

Table 1. The mechanism of HER in alkaline and acidic media.....	15
Table 2. Stoichiometric names of as-prepared samples.....	29
Table 3. The catalysts show varying Tafel slopes.	43
Table 4. C_{dl} values of different composites.	45
Table 5. R_{ct} and R_s values of catalyst in 1M KOH.	48

List of abbreviations

No.	Abbreviation	Full Name	No.	Abbreviation	Full Name
1	SOECs	Solid oxide electrolysis cells	11.	SEM	Scanning Electron Microscope
2.	WS	Water Splitting	12.	TEM	Transmission Electron Microscope
3.	OER	Oxygen Evolution Reaction	13.	HR-TEM	High Resolution Transmission Electron Microscope
4.	HER	Hydrogen Evolution Reaction	14.	CP	Chronopotentiometry
5.	ECWS	Electrochemical Water Splitting	15.	CV	Cyclic Voltammetry
6.	PEC	Photochemical Water Splitting	16.	LSV	Linear Sweep Voltammetry
7.	p-XRD	Powdered X-Ray Diffraction	17.	ECSA	Electrochemically Active Surface Area
8.	FTIR	Fourier Transform Infrared Spectroscopy	18.	EIS	Electrochemical Impedance Spectroscopy
9.	DSC	Differential Scanning Calorimetry	19.	TOF	Turn Over Frequency
10.	EDS	Energy Dispersive X-Ray Spectroscopy			

Chapter 1: Introduction

1.1. Energy Crisis

Energy is a critical component of modern society, powering businesses, transportation, and daily life. However, global reliance on fossil fuels like coal, oil, and natural gas, as well as renewables like wind, solar, and hydropower, has increased over time [1]. However, as the world's population has grown, energy requirements have increased, culminating in an energy shortage with long-lasting consequences for the environment, the economy, and society [2]. The Russian invasion of Ukraine in early 2022 hampered the rebound of global energy consumption from the pandemic-induced fall in 2020. The battle increased price pressures and hampered economic growth. Although market pressures existed prior to the invasion, the crisis amplified them, resulting in dramatic volatility and rapid spikes in energy prices, particularly natural gas in European markets. The threat of further supply disruptions continues to loom large. Despite the turbulence, renewable energy development has proven resilient. The crisis has caused several countries to reconsider their energy security requirements, resulting in fragmented energy connections with Russia that were once based on trust and reliability. This trend is changing global energy trade and investment patterns. As a result, countries are adopting steps to improve energy security, such as investing in domestic manufacturing capabilities in crucial areas [3]. A major question persists: will the current crisis hasten energy changes, or will financial turmoil and reactive policies hold them down? Record-high fossil fuel costs and growing emissions provide compelling reasons to abandon such fuels but worries regarding energy security may also drive further expenditures in fossil fuel infrastructure.

The energy crisis has emphasized global economies' vulnerability to variations in energy costs, with ramifications for both social and economic systems. Guan et al. (2023) highlighted the gravity of the situation in their analysis of 116 nations, which found that rising energy costs might result in a 62.6-112.9% increase in household expenditures. This dramatic increase imposes a substantial financial burden on millions of families, particularly those already on the verge of poverty. Low-income households spend a disproportionate share of their limited resources on energy bills, leaving less for vital needs like food, healthcare, and education [4]. These increasing expenses have a cascading effect that affects economies, rather than just individual people. Industries that rely on energy for generation, including manufacturing and agriculture, incur greater operational costs, frequently passed on to

consumers through increased product pricing. This cycle promotes inflation while reducing purchasing power, disproportionately hurting the most vulnerable communities. According to Guan et al. (2023), rising energy costs might push 78 to 141 million people into extreme poverty, putting further strain on social safety nets and exacerbating global inequality. In dealing with this situation, tailored energy aid programs have become critical. These programs seek to protect vulnerable communities from the immediate effects of increased energy prices while also encouraging equal access to critical resources. For example, direct energy bill subsidies can provide immediate support to needy households, ensuring that people are not forced to choose between heating their homes and putting food on the table. Similarly, measures that limit energy prices during periods of market volatility can help stabilize costs and keep rapid changes from wreaking havoc on both consumers and enterprises.

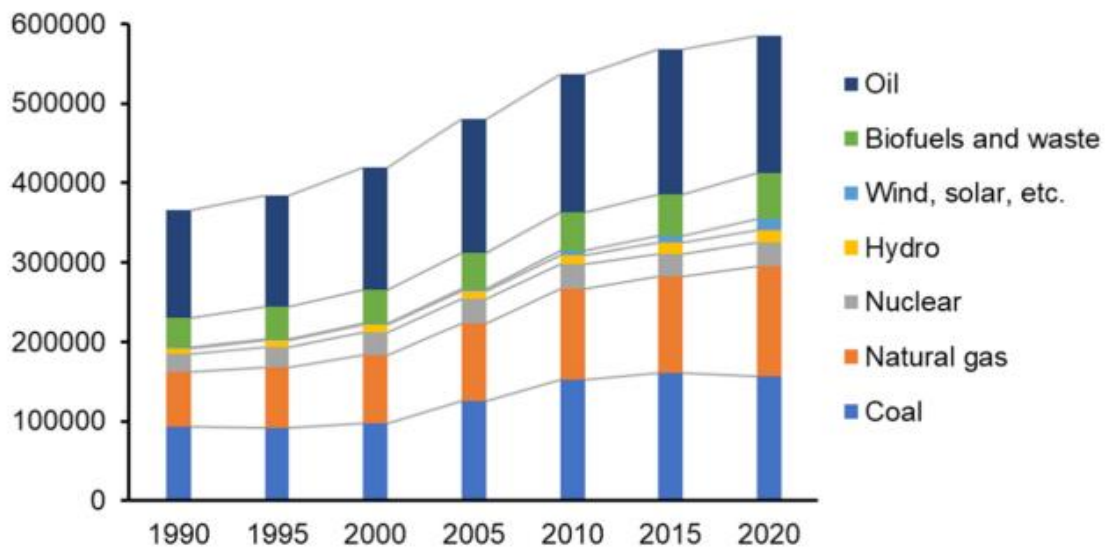
Another key part of crisis management is investing in long-term solutions to lessen reliance on fluctuating energy markets. Community-based renewable energy initiatives, such as solar cooperatives and small-scale wind farms, provide a sustainable and inclusive solution. These programs, which allow communities to create and control their own energy, not only reduce financial strain on homes but also contribute to larger efforts to decarbonize energy networks. These localized solutions can greatly enhance living standards and stimulate economic growth in emerging economies, where access to modern energy infrastructure is frequently limited.

Enhancing energy efficiency is an important part of tackling the situation. Governments and organizations can incentivize the use of energy-saving technologies like LED lighting, energy-efficient appliances, and enhanced insulation. These steps minimize energy usage, utility bills, and greenhouse gas emissions, resulting in a win-win situation for both households and the environment [5]. In addition, international cooperation is critical in addressing the global elements of the energy crisis. Wealthier nations, with their superior technologies and resources, bear a responsibility to assist emerging economies in moving to sustainable energy systems. This can be accomplished through financial aid, technology transfer, and initiatives to build capacity that enable municipalities and neighborhoods to undertake renewable energy projects and increase energy access.

The energy crisis provides a chance to address long-standing disparities and systemic weaknesses. Policymakers may promote social equality and ensure that no one is left behind by putting marginalized populations first in energy assistance initiatives. Targeted support for

rural regions, where biomass is commonly used for cooking and heating, can help to minimize deforestation, improve air quality, and improve general quality of life. Similarly, incorporating gender-sensitive measures into energy policies can empower women, who are frequently disproportionately affected by energy poverty, by giving them access to contemporary energy solutions and economic prospects.[6]

a Energy supply (EJ, thousands)



b Energy consumption (EJ, thousands)

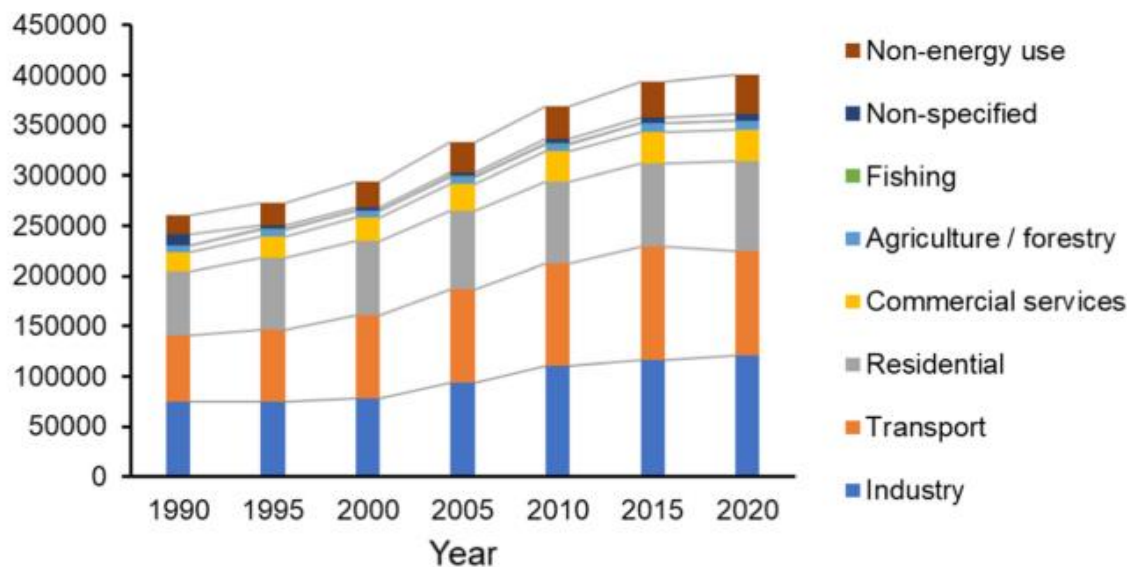


Figure 1. Energy supply from 1990 to 2020. a) Energy supply and b) Energy consumption. EJ: extra joules.[6]

To summarize, the energy crisis has highlighted the interconnection of energy, the economy, and society, emphasizing the critical need for comprehensive and equitable solutions.

While growing energy prices have grave immediate consequences, they also provide an opportunity for governments, organizations, and individuals to rethink and change energy systems to achieve a more sustainable and inclusive future. By fostering specific support, renewable energy, and energy efficiency, the global community can alleviate the current crisis while also laying the groundwork for future resilience. Guan et al.'s findings are both a frightening reminder of the stakes involved and a call to action to solve the issue with immediacy and compassion.

1.2. Challenges

The worldwide population has surpassed seven billion and is expected to reach nine billion by the middle of the century more than tripling present energy demand [7]. This rising need emphasizes the importance of creating renewable energy supplies, as nonrenewable energy sources will eventually be depleted. Hydrogen, the most plentiful element in the universe, has significant potential as a renewable energy source due to its clean burning, which yields only water as a byproduct [8]. Furthermore, hydrogen is substantially more efficient than traditional fuels, providing 2.5 times more energy per unit mass. However, industrial hydrogen production currently relies largely on nonrenewable energy, making it difficult to produce cost-effective and highly efficient hydrogen production from renewable energy sources.

1.3. Hydrogen as a promising solution

Today, hydrogen is primarily produced through high-temperature thermal processes, such as steam reforming or coal gasification. Electrical energy can be used to electrolyze water into hydrogen as a carbon-free energy source, although this method currently accounts for approximately 4% of worldwide hydrogen production, compared to more than 90% created through thermal processes. Recently, there has been an increasing interest in harnessing photonic energy to produce hydrogen. Solar hydrogen production uses sunlight to directly split water, utilizing the planet's vast solar and water resources to create a clean, endless fuel for a variety of purposes. Furthermore, biochemical energy provides another method for hydrogen production by utilizing microorganisms to transform biomass via biological processes such as dark fermentation, photo fermentation, and bio photolysis. Currently, thermal and electrical energy, primarily derived from fossil fuels, dominate hydrogen generation. However, as fossil fuel supplies grow rarer and more expensive throughout human lifetimes, a shift to renewable energy sources will be unavoidable. These renewable sources can offer the thermal, electrical, photonic, and biological energy required for long-term hydrogen production

1.4. Sources of hydrogen production

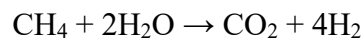
Hydrogen, as a versatile energy carrier, can be produced from a wide range of sources and processes. These methods are typically classified based on the primary energy input and the environmental impact of the production process. Below is an in-depth discussion of the key sources of hydrogen:

1. Fossil Fuel-Based Hydrogen

Fossil fuels remain the dominant source of hydrogen production, particularly due to their established infrastructure and high energy density. These methods are often categorized under "gray" or "blue" hydrogen, depending on the carbon management strategy.

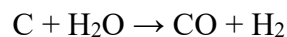
a. Natural Gas Reforming (Steam Methane Reforming - SMR)

It involves reacting natural gas (methane) with steam at high temperatures (700–1,000°C) to produce hydrogen and carbon dioxide. It is mature and widely used technology. It is cost-effective with existing natural gas infrastructure. However, it causes high carbon dioxide emissions unless carbon capture and storage (CCS) are implemented, in which case it is termed blue hydrogen.



b. Coal Gasification

Coal reacts with oxygen and steam under high pressure and temperature to produce a mixture of hydrogen, carbon monoxide, and carbon dioxide. It is potentially large-scale production in coal-rich regions. However, it causes high greenhouse gas emissions. It also requires advanced CCS to minimize environmental impact [9].



c. Oil Reforming

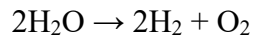
Hydrogen is extracted from crude oil or refinery byproducts through reforming processes. It is often integrated within petroleum refining industries to produce hydrogen for desulfurization and cracking processes.

2. Electrolysis of Water

Electrolysis is a promising and sustainable method for hydrogen production when powered by renewable energy sources. This is the basis for green hydrogen.

a. Alkaline Electrolysis (AEL)

Water is split into hydrogen and oxygen using an alkaline electrolyte such as potassium hydroxide. It is mature and reliable technology. It lowers capital cost compared to some other electrolyzer technologies. However, it is less efficient than emerging technologies like PEM.



b. Proton Exchange Membrane (PEM) Electrolysis

Uses a solid polymer electrolyte to conduct protons, with water splitting into hydrogen and oxygen. Higher efficiency and quicker response times compared to alkaline electrolysis. Compact and scalable for decentralized hydrogen production. High cost of materials (e.g., platinum for electrodes).

c. Solid Oxide Electrolysis Cells

It operates at high temperatures (700–1,000°C) using solid oxide materials as electrolytes. It is highly efficient due to the utilization of heat in the process and requires high-temperature-resistant materials.

3. Biomass and Biohydrogen

Hydrogen can be derived from renewable biomass sources, providing a carbon-neutral alternative.

a. Biomass Gasification

Biomass (e.g., wood, agricultural residues) is converted into hydrogen, carbon monoxide, and methane under high temperatures in the presence of oxygen or steam. It is renewable and widely available feedstock. It reduces waste by utilizing organic residues. However, it has high processing costs, and complicated feedstock preparation.

b. Anaerobic Digestion and Biophotolysis

Organic waste is decomposed by bacteria to produce biogas, which can be further processed to extract hydrogen. Photosynthetic microorganisms (algae, cyanobacteria) split water to produce hydrogen using sunlight. It is sustainable and eco-friendly processes. However, it causes low efficiency of the biological system and requires extensive research for scalability.

4. Renewable Energy-Driven Hydrogen

When hydrogen production is powered by renewable sources, it significantly reduces the carbon footprint.

a. Solar Hydrogen

It utilizes electricity generated from solar panels to power electrolysis units. It includes photoelectrochemical water splitting, which directly converts solar energy into chemical energy, splitting water into hydrogen and oxygen. Zero emissions during production. High compatibility with decentralized systems. Limited by sunlight availability and weather conditions.

b. Wind Hydrogen

Electricity generated from wind turbines powers electrolyzers for hydrogen production. Abundant and scalable in wind-rich regions. Dependence on consistent wind patterns [9].

5. Nuclear Hydrogen

Hydrogen is produced using the heat generated from nuclear reactors to drive high-temperature electrolysis or thermochemical cycles. High energy density and reliable output. Low operational carbon emissions. Public perception and safety concerns. High upfront costs for reactor construction.

6. Industrial Byproducts

Hydrogen can be recovered as a byproduct from various industrial processes, such as:

- **Chlor-Alkali Industry:** Produces hydrogen during the electrolysis of saltwater to generate chlorine and sodium hydroxide.
- **Refineries and Petrochemicals:** Hydrogen is often a secondary product of chemical reactions, including cracking and reforming.

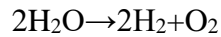
1.5. Future Trends and Innovations

Methane Pyrolysis is a low-emission technology that converts methane into hydrogen and solid carbon without producing CO₂. New electrolysis methods allow for direct hydrogen synthesis from seawater, eliminating the need for desalination. Ammonia may be cracked to produce hydrogen, useful for long-term storage and transport. Finally, hydrogen can be obtained through a variety of methods, each with its own set of benefits and drawbacks. Hydrogen production methods are chosen based on geographical resources, infrastructure, and

environmental goals. A shift to green and renewable hydrogen sources will be vital for achieving a low-carbon energy future [10].

1.6. Water splitting

Water splitting is the decomposition of water (H₂O) into its fundamental components, hydrogen (H₂) and oxygen (O₂). The chemical reaction is given by the equation:



The method is of great scientific and industrial interest because of its potential to produce hydrogen, a clean and sustainable energy carrier. Water splitting, on the other hand, is an energy-intensive reaction because water is thermodynamically stable, and dissociating water molecules requires overcoming significant energy barriers.

1.6.1. Thermodynamics of Water Splitting

The total water-splitting reaction is endergonic, which means it requires energy to proceed. Under typical conditions, water splitting has a Gibbs free energy change (ΔG) of roughly 237.2 kJ/mol, showing that the process is not spontaneous. This energy is equivalent to the energy necessary to break the strong O-H bonds in water molecules.

$$E^\circ = \Delta G^\circ / nF = 1.23 \text{ V}$$

Where:

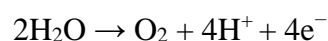
- n is the number of electrons transferred (4 for water splitting),
- F is Faraday's constant (96,485 C/mol).

However, due to inefficiencies and losses such as overpotentials, practical systems require higher voltages, typically around 1.8–2.0 V.

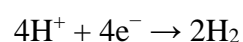
1.6.2. Chemical Pathway

Water splitting involves two half-reactions occurring at separate electrodes in an electrochemical cell:

- a) **Oxidation at the Anode (Oxygen Evolution Reaction):** At the anode, water molecules lose electrons and are oxidized to produce oxygen gas. This reaction is kinetically slow and energy-intensive due to the multiple proton-coupled electron transfer steps and the formation of O=O bonds.



- b) **Reduction at the Cathode (Hydrogen Evolution Reaction):** At the cathode, protons (H⁺) are reduced by gaining electrons to form hydrogen gas. This reaction is relatively faster but still requires a suitable catalyst to achieve efficient electron transfer.



1.6.3. Mechanistic insights

The effectiveness of water splitting is determined by assisting the bond-breaking and bond-forming phases via catalysis. Catalysts are utilized to reduce energy activation and increase reaction rates in both OER and HER. The selection of catalysts is crucial for the following reasons. For OER, the catalyst must stabilize high-energy intermediates like hydroxyl radicals (OH^*) and peroxides (O-OH^*). For HER, the catalyst should promote hydrogen adsorption and recombination. Intermediate processes involve the formation of hydroxide (OH^-) or hydronium (H_3O^+) ions based on pH.

Steps for proton-coupled electron transfer

- Formation and desorption of gas molecules (H_2 and O_2) on electrode surfaces.
- To get around energy obstacles, more voltage above the thermodynamic barrier is required, particularly for OER due to its complex multi-electron process. Efficient electron transport at electrode surfaces is crucial for reducing energy loss.

1.6.4. Factors affecting Water Splitting:

- Mass Transport:** The dispersion of reactants (water) and elimination of products (H_2 and O_2) affect overall efficiency.
- pH of electrolyte:** In acidic media, water dissolves into H_3O^+ ions. In alkaline environments, water dissociates into OH^- ions. Both influence reaction routes and catalyst choices.
- Electrode Material:** - Catalysts such as platinum (for HER) and transition metal oxides (for OER) are commonly employed to improve efficiency.
- Energy Input:** Depending on the system design, energy can be delivered by electrical, thermal, or light sources.

Water splitting has enormous potential as a clean hydrogen generation technology because it emits zero carbon dioxide when fueled by renewable energy sources. The scientific challenge is to find cost-effective, efficient, and long-lasting materials to reduce energy consumption and boost the scalability of this vital process.

1.7. Types of water splitting:

Water splitting is a thermodynamically difficult reaction that requires an external energy input to progress, whereas the reverse reaction happens quickly. Hydrogen can be created utilizing a variety of energy sources, including renewable and nonrenewable resources. Figure 1 depicts various water-splitting methods powered by thermal, electrical, photonic, and biochemical energy via processes such as thermolysis, electrolysis, photolysis, and biolysis.

Furthermore, hydrogen generation can use combinations of various energy types in hybrid systems, which are often more thermodynamically advantageous than non-hybrid approaches. Hybrid systems combine energy sources such as thermal and electrical, electrical and photonic and photonic and biochemical. Hybrid systems lower expenses for operation, minimize activation barriers, improve reaction kinetics, and raise hydrogen production rates by replacing some of the needed power with less expensive or renewable resources. Recent advances in catalytic technology have also resulted in substantial progress in developing technologies for producing hydrogen, including electrocatalytic, photocatalytic, photoelectrochemical, and photobiological water splitting. Furthermore, nuclear energy is used in water dissociation, in which nuclear (mainly alpha) radiation divides water into hydrogen and hydroxyl radicals. These radicals are very reactive and recombine to generate other reactive species, including superoxide (HO_2) and peroxide (H_2O_2), which contribute to further chemical processes.

1.7.1. Photocatalytic water splitting

Photocatalytic water splitting is a chemical reaction that uses sunshine to break down water (H_2O) into its basic atoms of hydrogen (H_2) and oxygen (O_2). This process has received widespread attention as a sustainable and environmentally beneficial way to manufacture hydrogen, a clean and renewable energy carrier that addresses global energy and environmental concerns [11].

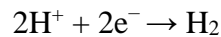
Key Elements of Photocatalytic Water Splitting

- 1. Photocatalyst:** A substance that absorbs sunlight and uses its energy to accelerate a reaction. Ideal photocatalysts have a band gap of 1.8-3.2 eV, can absorb visible or ultraviolet light, are chemically stable in aqueous settings, and efficiently separate and migrate photogenerated electron-hole pairs. Common materials include titanium dioxide (TiO_2), zinc oxide (ZnO), cadmium sulfide (CdS), and emerging materials like metal-organic frameworks (MOFs) and perovskites.
- 2. Light Source:** Solar energy is the primary source used in the procedure. The wavelength and intensity of light influence the reaction's efficiency. Water is the source of hydrogen and oxygen.
- 3. Reaction Sites:** The catalyst should have active sites for the hydrogen and oxygen evolution reaction [12].

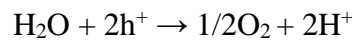
Mechanism for Photocatalytic Water Splitting

- ❖ **Photon Absorption:** When a photocatalyst absorbs photons with equal or greater energy than its band gap, electrons (e^-) in the valence band are driven to the conduction band, leaving holes (h^+) in the valence band.
- ❖ **Charge Separation and Migration:** Photogenerated electrons and holes move to the photocatalyst's surface, preventing recombination. Achieving great efficiency requires effective charge separation.
- ❖ **Reduction and Oxidation Reactions:**

- The electrons participate in the reduction reaction to produce hydrogen:



- The holes drive the oxidation reaction to produce oxygen:



These reactions occur simultaneously on the photocatalyst's surface.

Challenges

- Photocatalysts often have low efficiency due to poor light absorption and rapid electron-hole recombination.
- Photocatalysts, such as TiO_2 , primarily absorb UV light, which accounts for just a small portion of solar radiation.
- Photocatalysts can degrade during reactions, particularly in acidic or basic conditions.
- Creating cost-effective and scalable solutions is tough.

Recent Advances

1. Bandgap Engineering involves modifying photocatalysts to absorb visible light through doping with nonmetals (e.g., nitrogen, sulphur) or metals (e.g., transition metals).
2. Combining multiple materials to improve charge separation and light absorption, such as TiO_2/CdS heterojunctions.
3. Using co-catalysts, such as platinum or nickel, enhances reaction kinetics by creating active sites for HER or OER.
4. Creating nanomaterials with large surface areas to improve light absorption and reaction efficiency.

Applications for Photocatalytic Water Splitting

- **Hydrogen Production:** A renewable source for fuel cells, industrial uses, and energy storage.

- **Environmental benefits:** Reduces reliance on fossil fuels and lowers greenhouse gas emissions.
- **Integration of Renewable Energy Systems: Combining** with solar panels or other renewable energy sources to produce decentralized and sustainable hydrogen. Photocatalytic water splitting is a potential technique for the hydrogen economy, but further study is needed to address efficiency, stability, and scalability issues. With advances in materials science and engineering, it has the potential to transform sustainable energy generation [13-15].

1.7.2. Photoelectrochemical water splitting

Photoelectrochemical water splitting is the process of decomposing water into hydrogen and oxygen utilizing electrical charges specifically, photogenerated electron-hole pairs within catalysts under light irradiation. This method combines electrochemical water splitting with light absorption, with photogenerated electrons driving water reduction to produce hydrogen and holes facilitating water oxidation to generate oxygen. Honda and Fujishima pioneered PEC water splitting in the 1970s, using TiO_2 as a photoanode and platinum as a counter electrode. This accomplishment spurred great interest to create various semiconducting metal oxides as photoanodes for PEC water splitting due to their low cost and resilience to photo corrosion.

Many of these materials are wide-bandgap metal oxides that need ultraviolet light to be excited to split water with PEC. Metal oxides that respond to visible light, such as WO_3 , Fe_2O_3 , and BiVO_4 , have low conduction band potentials, limiting their ability to reduce water and produce hydrogen. To address this problem, external bias is frequently added between the photoanode and counter electrode, allowing these oxide semiconductors to work successfully in PEC water splitting and thereby expanding their utility under visible light.

1.7.3. Photovoltaic-integrated photoelectrochemical (PEC) water splitting

Photovoltaic-integrated photoelectrochemical water splitting converts solar radiation into hydrogen by merging photovoltaic (PV) systems and water-splitting technology. Traditionally, a photovoltaic system converts solar energy into electrical power, which is then utilized to operate an external electrolyzer for hydrogen synthesis. For example, an 18%-efficient crystalline silicon photovoltaic system combined with an 80%-efficient electrolyzer results in a solar-to-hydrogen conversion efficiency of about 14%. This efficiency can theoretically be increased when combined with higher-efficiency PV systems. Because the PV system and electrolyzer are built independently, the solar cells stay outside the electrolyte, thus rendering them immune to corrosion. This design uses sustainable solar energy to produce hydrogen

without generating greenhouse gases, assuring long-term durability. Solar photovoltaics, however, continue to be limited by their high production and installation costs. To overcome this issue, an alternate method combines the solar device and electrolyzer into a single unit. This integration reduces costs and avoids mechanical problems associated with the separate manufacture and connecting of solar cells and electrochemical systems.

Integrated devices often have light absorbers made up of single or many connections. Tandem designs (multiple connections) stack light absorbers with variable band gaps to make better use of the solar spectrum and generate more photopotential. Alternatively, connecting multiple single-junction cells in series allows for the efficient utilization of narrow bandgap absorbers, increasing solar light absorption while retaining the necessary photopotential for water splitting.

1.7.4. Introduction to Electrochemical water splitting:

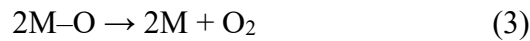
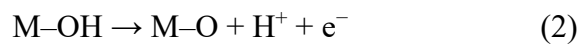
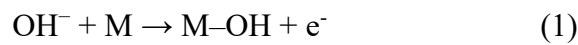
Since the early 1900s, commercial water electrolysis has produced around 4% of today's hydrogen production [16]. This water splitting technique is technologically easy, but its commercial impact is limited due to high energy consumption. Electrocatalysts are added to the anode and cathode to catalyze the electrocatalytic water reduction and oxidation reactions, respectively, to increase the reaction kinetics and efficiency of water electrolysis. Noble metals are now routinely used as electrocatalysts for water splitting. Ir [17] and Ru [18] as well as their oxides [19], are used at the anode to increase OER for the water oxidation process, whereas Pt, a well-known hydrogen evolution catalyst, is used at the cathode to increase HER for the water reduction reaction.

1.8. Mechanism of Oxygen Evolution Reaction

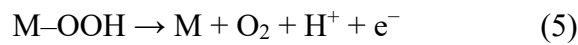
The oxygen evolution process in alkaline water splitting takes place on the surface of metal sites, designated by M. Several theories have been proposed over the years to explain the OER process in acidic and alkaline environments, showing both parallels and differences. Most methods use common intermediates like MOH, MO, and MOOH, with changes mostly occurring in the step that produces molecular oxygen. Oxygen can be produced directly from the conjunction of two MO intermediates or by forming and then transforming a MOOH intermediate. The bonding strength (M-O) between these intermediates and the metal active sites is a significant component influencing OER activity, as it has a direct impact on the catalyst's overall electrochemical performance [20].

The typical OER mechanism consists of multiple phases, each requiring electron and proton exchanges. Initially, hydroxide ions (OH^-) get absorbed onto the active site and oxidized to create MOH. The M-OH species is then oxidized to M-O. At this point, oxygen can originate via two different mechanisms. One method is to mix two nearby M-O species to produce O_2 , which regenerates the active sites. The other is when M-O is changed to M-OOH via further oxidation, subsequently followed by another electron-proton transfer that releases O_2 and re-exposes the active site [21]. The following equations describe what happens at the cathode and anode undergoing OER in alkaline media:

Pathway 1:



Pathway 2:



Thermodynamic modelling of OER has gotten a lot of attention, with an emphasis on the reaction energy for each elementary step. The adsorption energies of the intermediates (M-OH, M-O, and M-OOH) fluctuate irregularly and determine the reaction's free energy profile. The step with the freest energy is designated as the rate-determining phase. The binding energies between active metal sites and intermediates play an important role in the effectiveness of OER catalysts [22]. For example, high M-O binding can limit M-OOH formation, whereas weak M-O binding makes M-O formation more difficult. Studies indicate that materials like $\beta\text{-MnO}_2$ have moderate oxygen binding energies, allowing for direct O-O recombination. These insights have been instrumental in understanding and optimizing the catalytic behavior of OER systems [23].

1.9. Mechanism of Hydrogen Evolution Reaction

The electrochemical hydrogen evolution reaction (HER) has separate reaction mechanisms in both alkaline and acidic media, but the first stage, defined as the Volmer reaction (electrochemical adsorption), is shared by both. During this process, electrons supplied to the electrode surface (M) via an external circuit enable protons from the solution to be adsorbed,

resulting in adsorbed hydrogen (H_{ads}). In acidic media, protons (H^+) are drawn straight from the solution. In alkaline media, H_{ads} is generated by releasing OH^- ions from adsorbed water molecules. The second step includes the production of molecular hydrogen (H_2), which can be accomplished via either the Heyrovsky or Tafel reactions [24]. Under conditions of low H_{ads} coverage, the Heyrovsky reaction dominates, where H_{ads} combines with a proton from the solution and an electron from the external circuit to form H_2 . On the other hand, if the Volmer reaction proceeds rapidly, resulting in higher H_{ads} coverage, the Tafel reaction occurs, wherein two adjacent H_{ads} atoms combine to generate H_2 .

Table 1. The mechanism of HER in alkaline and acidic media.

Media	Volmer reaction	Heyrovsky reaction	Tafel reaction
Alkaline	$H_2O + e^- \rightarrow H_{\text{ads}} + OH^-$	$H_{\text{ads}} + H_2O + e^- \rightarrow H_2 + OH^-$	$2H_{\text{ads}} \rightarrow H_2$
Acidic	$H^+ + e^- \rightarrow H_{\text{ads}}$	$H^+ + e^- \rightarrow H_{\text{ads}}$	$2H_{\text{ads}} \rightarrow H_2$

The Gibbs free energy shift of hydrogen adsorption (ΔGH^*) is a significant component regulating HER catalytic performance as it assesses the ease of adsorption and desorption. An ideal ΔGH^* near to zero allows hydrogen atoms to easily adsorb onto the catalyst surface and desorb to create H_2 . Volcano plots of ΔGH^* reveal Fe, Co, and Ni-based electrocatalysts as viable alternatives to Pt for HER. The fibrous shape of catalysts improves electron transport and conductivity, increasing HER performance. As a result, nanofiber-structured transition metals, alloys, and their phosphides, sulphides, and selenides have received a lot of attention as effective HER catalysts [25].

Both OER and HER face efficiency challenges due to factors like slow reaction kinetics, recombination of intermediates, and the stability of catalysts under operational conditions. Strategies to address these include engineering the electronic and structural properties of catalysts, introducing dopants to modify active sites, and designing nanostructured materials to increase surface area and improve reaction rates. Together, advancements in understanding the fundamental mechanisms and developing efficient catalysts are critical to enhancing the performance of these reactions and achieving scalable hydrogen production [26, 27].

1.10. Fundamental Electrochemistry of Water Splitting

Electrocatalysts' performance in water splitting is evaluated using important characteristics and methodologies, including overpotential (η) at different current densities, Tafel slope, turnover

frequency, and stability. These parameters, which are briefly detailed below, provide vital insights into the efficiency and durability of electrocatalysts.

1. Overpotential (η):

Overpotential is the extra potential (voltage) required beyond the thermodynamic equilibrium potential of a reaction to drive it at a given rate. In water splitting, the equilibrium potential for the hydrogen evolution reaction (HER) is 0 V (vs. reversible hydrogen electrode, RHE). For the oxygen evolution reaction (OER), it is 1.23 V (vs. RHE) [28].

➤ **Why Overpotential Matters:**

- Indicates the efficiency of a catalyst. Lower overpotentials suggest a more efficient catalyst.
- Measured at a defined current density (e.g., 10 mA/cm², a benchmark for water splitting).

➤ **Factors Affecting Overpotential:**

- Activation energy of the reaction.
- Catalyst material and surface properties.
- Reaction kinetics (e.g., adsorption and desorption of intermediates).

2. Tafel Slope:

The Tafel slope is derived from the Tafel equation:

$$\eta = b \log(j) + a \quad (6)$$

Where, η refers to overpotential, j corresponds to the current density, and b relates to the Tafel slope, representing the rate of increase in overpotential with current density.

➤ **Why Tafel Slope Matters:**

- Provides insight into the reaction kinetics and the rate-determining step (RDS).
- A lower Tafel slope indicates faster charge transfer and better catalytic performance [29].

➤ **Typical Tafel Slopes for HER and OER:**

- **For HER:**
 - 120 mV/decade: Volmer step (adsorption) is rate-determining.

- 40 mV/decade: Heyrovsky or Tafel step (desorption or recombination) is rate-determining.
- **OER:**
 - Slopes vary depending on the reaction mechanism and catalyst material, often between 40–120 mV/decade.

3. Turnover Frequency (TOF):

TOF is the number of catalytic cycles per active site per unit time, often expressed as:

$$\text{TOF} = \text{Number of molecules transformed} / \text{Number of active sites} \times \text{Time}$$

➤ Why TOF Matters:

- Quantifies the intrinsic activity of a catalyst, independent of surface area or loading.
- High TOF values indicate that each active site is highly efficient.

➤ Calculation of TOF:

- Requires knowledge of the total active sites, often determined using electrochemical techniques (e.g., double-layer capacitance or specific adsorption methods) [30].

➤ Units:

- Typically given in s^{-1}

4. Stability Evaluation:

Stability is crucial for practical applications of catalysts. It assesses the catalyst's durability and resistance to degradation under operating conditions [31].

1. **Chronopotentiometry/Chronoamperometry:** Measures potential or current over time at a fixed current density or potential. A stable potential or current indicates good stability.
2. **Cycling Tests (Cyclic Voltammetry):** Cycles the potential repeatedly between set limits to mimic real operating conditions. Degradation in current density or increase in overpotential over cycles suggests poor stability.
3. **Post-Characterization:** Analyzing the catalyst before and after testing (e.g., XRD, SEM, TEM, XPS) to observe structural or compositional changes.

4. **Gas Evolution Monitoring:** Quantifies H₂ and O₂ production over time using gas chromatography or mass spectrometry. Consistent gas evolution rates indicate stable performance.

Common Degradation Issues:

- Catalyst dissolution or oxidation.
- Loss of active sites due to surface reconstruction.
- Agglomeration or detachment of catalyst particles.

By analyzing these parameters comprehensively, researchers can determine the performance, efficiency, and feasibility of catalysts for electrochemical applications like water splitting.

1.11. Electrochemistry involved in EWS

Electrochemical techniques like Cyclic Voltammetry, Linear Sweep Voltammetry, Electrochemical Impedance Spectroscopy, Chronopotentiometry, and Electrochemical Surface Area measurements play critical roles in understanding and optimizing water-splitting processes.

- **Cyclic Voltammetry**

CV is widely used to study the redox responses of electrocatalysts, delivering data regarding surface-active sites along with catalyst stability. CV examines redox transitions, including variations in states of oxidation (e.g., Co²⁺ → Co³⁺ → Co⁴⁺ in cobalt-based catalysts), to better comprehend reaction pathways for the oxygen evolution reaction as well as hydrogen evolution reaction. It also assesses catalyst stability over extended durations of cycling.

- **Linear Sweep Voltammetry**

LSV is a fundamental technique to assess catalytic activity by measuring the overpotential required to achieve a specific current density. This method highlights the onset potential and enables the comparison of the intrinsic activity of different catalysts.

A lower overpotential and a steeper current increase in LSV curves indicate a more efficient electrocatalyst. Meanwhile, EIS provides valuable information about charge transfer resistance (R_{ct}) and ion transport processes. By analyzing Nyquist plots, researchers can deduce kinetic and diffusion-controlled processes, where a lower R_{ct} signifies improved charge transfer and higher catalytic performance.

- **Chronopotentiometry**

To evaluate long-term stability, Chronopotentiometry and Chronoamperometry are employed, monitoring potential or current over time at constant current or potential, respectively. Stable readings indicate the durability of the catalyst during HER and OER operations.

- **Electrochemically Active Surface Area**

Lastly, ECSA measurements determine the active surface area of a catalyst, which is directly proportional to the number of exposed active sites. This metric, determined from double-layer capacitance (Cdl) in non-faradaic CV areas, is critical for normalizing and comparing electrocatalyst intrinsic activity levels.[32]

Collectively, these methodologies provide a thorough understanding of catalyst performance, ranging from kinetics and stability to active site accessibility and reaction processes. Integrating these insights allows researchers to create and optimize electrocatalysts for efficient and long-lasting water-splitting applications.[33]

1.12. Spinel structures as electrocatalyst for WS

Spinel is a class of minerals and synthetic materials with a distinctive crystalline structure that belongs to the cubic crystal system. Their general chemical formula is AB_2O_4 , where A and B represent different metal cations, and O denotes oxygen anions. The A^{2+} cation typically occupies tetrahedral sites, while the B^{3+} cations are distributed over octahedral sites within the lattice. Spinel is known for its robust structural stability, diverse compositions, and remarkable physical and chemical properties, making it valuable in numerous scientific and industrial applications.

1.12.1. Structure of Spinel

The spinel structure is based on a closely packed cubic arrangement of oxygen anions, with cations occupying interstitial sites. The arrangement can be visualized as follows:

- **Tetrahedral sites:** These are smaller and are occupied by A-site cations (commonly divalent, such as Mg^{2+} , Zn^{2+} , or Fe^{2+}).
- **Octahedral sites:** These are larger and accommodate B-site cations (commonly trivalent, such as Al^{3+} , Fe^{3+} , or Cr^{3+}).

The precise distribution of cations in tetrahedral and octahedral sites determines the type of spinel:

1. **Normal spinels:** The A-site cations exclusively occupy tetrahedral sites, while B-site cations are found in octahedral sites. Example: MgAl_2O_4 (magnesium aluminate).
2. **Inverse spinels:** Half of the B-site cations occupy tetrahedral sites, while the A-site cations and the remaining B-site cations occupy octahedral sites. Example: Fe_3O_4 (magnetite).
3. **Mixed spinels:** A fractions of A and B-site cations are randomly distributed over tetrahedral and octahedral sites.

1.12.2. Examples of Spinel

Natural and synthetic spinels exhibit a wide range of compositions and applications.

- **Natural Spinel:** Found in mineral deposits, often as gemstones or ores. Examples include chromite (FeCr_2O_4) and spinel gemstones (MgAl_2O_4).
- **Synthetic Spinel:** Created for specific applications, such as ferrites ($\text{M}_x\text{Fe}_{3-x}\text{O}_4$, where M is a metal cation) for magnetic and electronic devices.

1.12.3. Properties of Spinel

1. **Structural Stability:** Spinel exhibit high thermal and mechanical stability, making them suitable for refractory applications.
2. **Electrical and Magnetic Properties:** Depending on the composition, spinels can be insulators, semiconductors, or exhibit magnetic behavior (e.g., ferrimagnetism in magnetite).
3. **Optical Properties:** Transparent spinels are used as optical materials or gemstones.

1.12.4. Applications for Spinel

1. **Catalysis:** Spinel, particularly transition metal spinels, are widely used as catalysts or catalyst support in various chemical reactions, including water splitting, oxidation, and reduction processes.
2. **Magnetic Materials:** Ferrite spinels (e.g., NiFe_2O_4 , CoFe_2O_4) are essential in magnetic data storage and electromagnetic devices.
3. **Refractory Materials:** Due to their high melting points and stability, spinels are used in furnaces and as linings in kilns.
4. **Electrochemical Devices:** Spinel are used as electrode materials in batteries, supercapacitors, and fuel cells due to their favorable electrochemical properties.
5. **Optical and Decorative Uses:** Transparent spinels are utilized in lasers, lenses, and as synthetic gemstones.

1.13. CoGa₂O₄ as an electrocatalyst

The oxygen evolution reaction (OER) via electrocatalysis is based on the redox shifting of active species. The quiescent state of cobalt-based oxygen evolution catalysts (OECs) is Co²⁺/Co³⁺. High overpotential causes cobalt to oxidize to Co⁴⁺, an active site that interacts with OH⁻ to create O₂. Ideally, an OEC should generate an inhibitor environment that manages two conflicting factors: catalyst security, which calls for strong ion-constraining capacity, along with elevated catalytic activity, which demands active ions in a less limited environment. Because of their tight structural constraints, compact, extremely crystalline catalysts with strong lattice structures frequently exhibit sustained catalytic performance. However, such materials largely facilitate "surface catalysis," whereby water oxidation occurs only on the crystal surface and no ions penetrate the bulk. This reduces catalytic efficiency. Attempts to add porous structures into these materials to increase reactive surface areas have somewhat improved OER efficiency but fail to overcome inherent difficulties [34].

1.13.1. Advantages of using CoGa₂O₄

Cobalt gallium oxide (CoGa₂O₄) has emerged as a promising electrocatalyst for water splitting due to several advantageous properties:

- ❖ **Spinel Structure with Enhanced Stability:** CoGa₂O₄ adopts a spinel structure, which is known for its excellent chemical and structural stability. This stability ensures long-term durability in harsh operating environments, such as alkaline or acidic electrolytes, used in water splitting.
- ❖ **Optimal Electronic Properties:** The spinel structure facilitates efficient electron transport due to its mixed valency of cobalt ions (Co²⁺ and Co³⁺), which can participate in redox reactions. This enhances the oxygen evolution reaction kinetics.
- ❖ **High Surface Area and Porosity:** The ability to synthesize CoGa₂O₄ as porous or nanostructured materials increases the active surface area, providing more catalytic sites for HER and OER, thereby boosting overall activity.
- ❖ **Synergistic Effect of Cobalt and Gallium:** Cobalt acts as an active catalytic center for water splitting, while gallium provides a stabilizing framework. The incorporation of gallium reduces cobalt dissolution and stabilizes the structure during electrocatalysis, enhancing its operational lifespan.

- ❖ **Moderate Binding Energy for Reaction Intermediates:** CoGa_2O_4 has optimal binding energy for intermediates like OH^- , O^- , and OOH^- in the OER process. This enables efficient reaction pathways with lower overpotentials and better reaction kinetics.

1.13.2. Advantages of using NiGa_2O_4

Nickel gallium oxide (NiGa_2O_4) is a promising electrocatalyst for water splitting, offering several advantages due to its unique properties and synergistic effects of nickel and gallium [35].

- ❖ **High Stability and Robustness:** NiGa_2O_4 possesses a spinel structure, which provides excellent thermal, chemical, and structural stability under harsh operating conditions, such as high pH and temperature environments typical of water splitting processes. Gallium in the lattice enhances the stability of nickel ions, preventing catalyst degradation and maintaining performance over extended operation.
- ❖ **Enhanced Catalytic Activity:** Nickel ions (Ni^{2+} and Ni^{3+}) serve as active sites for the oxygen evolution reaction (OER) and hydrogen evolution reaction (HER), promoting efficient catalysis. The interaction between nickel and gallium enhances the catalytic properties by optimizing the electronic structure and reducing energy barriers for reaction intermediates.
- ❖ **Low Overpotential and Improved Kinetics:** NiGa_2O_4 exhibits low overpotentials for both OER and HER due to its ability to effectively adsorb and desorb reaction intermediates such as OH^- , O^- , and OOH^- for OER, and H^* for HER. The electronic properties of NiGa_2O_4 facilitate faster charge transfer, improving overall reaction kinetics.
- ❖ **High Surface Area and Porosity:** NiGa_2O_4 can be synthesized in nanostructured or porous forms, which increase the surface area and expose more active catalytic sites. This enhances the overall catalytic activity.
- ❖ **Optimal Binding Energy for Reaction Intermediates:** The binding energy of NiGa_2O_4 for reaction intermediates is close to the ideal value, ensuring efficient progression of water splitting reactions with minimized energy losses.

Chapter 2: Literature Review

Peng et al. (2021) [36] reviews strategies to enhance cobalt-based electrocatalysts for water splitting, focusing on both hydrogen evolution reaction (HER) and oxygen evolution reaction (OER). Key enhancement methods include morphology regulation to increase active sites, electrode structure design to improve electron/ion transport, and catalyst anchoring for better stability. Surface defects, elemental doping, and heterostructure interfaces are highlighted for their ability to modify electronic structures and boost catalytic activity. The authors emphasize the need to address challenges like catalyst stability, scalability, and efficiency. Future directions suggest advanced material designs and mechanistic studies to optimize cobalt-based catalysts for sustainable hydrogen production. This work provides a comprehensive guide for improving the performance of electrocatalysts in water splitting.

Zhang et al. (2020) [37] describe the development of void waxberry like cobalt-nickel oxide endorsed on sulphur and nitrogen-codoped carbon nanospheres (Co-NiO/S, N-CNS) as a trifunctional electrocatalyst for the oxygen evolution reaction (OER), oxygen reduction reaction (ORR), and hydrogen evolution reaction (HER). The peculiar hollow form creates several active sites and improves mass transfer, while S and N codoping increase electrical conductivity and catalytic efficiency. The material demonstrated significant electrocatalytic activity, low overpotentials for OER and HER, and excellent ORR performance. The study focusses on Co-NiO/S, N-CNS as an affordable and functional material for energy transformation applications including water splitting and fuel cells. This work focusses on the interaction between structural design and doping approaches in multifunctional electrocatalysis.

Wu et al. (2019) [38] describe a novel nickel-cobalt phosphite electrocatalyst featuring face-sharing octahedral frameworks for efficient water splitting. The material, which was developed utilizing a unique synthetic technique, exhibits improved electrocatalytic activity during the oxygen evolution reaction (OER) as well as the hydrogen evolution reaction (HER). The synergistic effects of nickel and cobalt, in addition to the structural benefits of face-sharing octahedra, allow for effective transfer of charge and many active sites. The catalyst has low overpotentials and excellent stability in alkaline environments, indicating its potential for use in water electrolysis. This research emphasizes the innovative design of transition metal-based phosphites as low-cost alternatives to noble metal-based electrocatalysts.

Duraivel et al. (2022) [39] reports the synthesis of a hierarchical 3D flower-like cobalt hydroxide structure as an efficient bifunctional electrocatalyst for water splitting. The unique morphology offers a high surface area, providing abundant active sites for the oxygen evolution reaction (OER) and hydrogen evolution reaction (HER). The catalyst exhibits low overpotentials and impressive catalytic stability in alkaline media, demonstrating excellent bifunctional performance. Structural characterization reveals that the hierarchical design facilitates superior charge transfer and gas bubble release, enhancing overall efficiency. This study underscores the potential of cobalt hydroxide-based materials as cost-effective and robust alternatives to noble metal-based electrocatalysts for sustainable energy applications.

Peng et al. (2015) [40] presents a research of homologous Ni-Co-based nanowires employed as complementary electrocatalysts for total water splitting, which includes both the oxygen evolution reaction (OER) and the hydrogen evolution reaction. The nanowires are produced using a scalable electrodeposition procedure, and their distinctive structure provides a large surface area and efficient charge transfer. Ni-rich nanowires have strong catalytic activity in OER, but Co-rich nanowires function well in HER. With these complimentary capabilities, the catalysts can attain minimal overpotentials for both reactions in alkaline media. The work emphasizes the potential of Ni-Co nanowires as cost-effective and durable electrocatalysts for sustainable water splitting applications.

Xu et al. (2016) [41] Investigate how crystallinity affects the water oxidation performance of mesoporous spinel CoGa_2O_4 . The study shows that changing the crystallinity of CoGa_2O_4 improves its catalytic efficiency in the oxygen evolution process (OER). The mesoporous structure, paired with controlled crystalline, results in an abundance of active sites, enhanced charge transport, and increased stability. The optimized CoGa_2O_4 shows low overpotential and high current density under alkaline circumstances, demonstrating its potential as an efficient and long-lasting OER electrocatalyst. This study emphasizes the need to adjust material crystalline to improve electrocatalytic performance in water-splitting applications.

Zhe Xu et al. (2016) [41] investigates the link between crystallinity and catalytic activity in oxygen evolution reactions (OER). The authors boosted electrocatalytic activity by carefully modifying the crystallinity of mesoporous CoGa_2O_4 . This resulted in higher charge transfer, active sites, and structural stability. The work emphasizes the advantages of combining a mesoporous design with optimized crystallinity, which results in lower overpotentials and

higher current densities under alkaline circumstances. This study emphasizes the importance of structural engineering in developing efficient and long-lasting catalysts for water oxidation.

SX Zhou et al., (2015) [35] reports the effective synthesis of NiGa_2O_4 octahedral nanocrystals with exposed (111) facets using a controlled hydrothermal technique. The (111) facets, with increased surface energy, significantly improve photocatalytic water-splitting efficiency. Structural and morphological analysis indicate the nanocrystals' distinctive facet exposure, high crystallinity, and enhanced surface area. Photocatalytic tests show that simulated sunlight significantly improves hydrogen evolution rates in NiGa_2O_4 compared to other morphologies. The (111) facets provide plentiful active sites, increased light absorption, and efficient charge separation, reducing electron-hole recombination. The findings emphasize the significance of facet engineering in photocatalyst design, giving a viable way to developing sustainable hydrogen production systems via photocatalysis.

Hun Xue et al., (2008) [42] describes the effective hydrothermal synthesis of hollow rods of nanocrystalline NiGa_2O_4 with Ga_2O_3 as a template. The study highlights crucial synthesis parameters, such as pH, reaction time, and temperature, that influence the product's phase and microstructure. A formation mechanism for the hollow rod shape is postulated, which involves a dissolution-precipitation process aided by hydrothermal conditions. The study expands on this process to create different hollow rod structures, including ZnGa_2O_4 , demonstrating its adaptability. Photocatalytic tests show that RuO_2 -loaded NiGa_2O_4 has higher activity in photocatalytic water splitting, making it a potential material for sustainable hydrogen production. These findings highlight the potential of hollow nanostructures in improving photocatalyst efficiency and scalability.

Xiao Jun Lv et al., (2016) [43] examines the photocatalytic efficacy of SnO_x - NiGa_2O_4 composites for water splitting during light irradiation. NiGa_2O_4 acts as the base photocatalyst, with SnO_x added to improve charge separation and catalytic efficiency. Structural and compositional investigations reveal good integration of SnO_x with NiGa_2O_4 , generating a heterojunction that efficiently separates electrons and holes. Photocatalytic measurements show that SnO_x - NiGa_2O_4 produces more hydrogen and oxygen than virgin NiGa_2O_4 . The synergistic impact of SnO_x and NiGa_2O_4 enhances light absorption, reduces recombination rates, and increases the number of active sites. The study examines the stability and reusability of the SnO_x - NiGa_2O_4 photocatalyst, demonstrating its consistent performance across numerous cycles.

Francesco Di Quarto et al., [44] use electronegativity differences between oxygen and the average electronegativity of the cations to model band-gap values. This method is used for ternary spinels (ZnAl_2O_4 , ZnGa_2O_4 , MgAl_2O_4 , and MgGa_2O_4), double spinels ($\text{Mg}(\text{Al}_{1-x}\text{Ga}_x)\text{O}_4$ and $\text{Zn}(\text{Al}_{1-x}\text{Ga}_x)\text{O}_4$), and quaternary mixed oxides ($\text{Zn}_x\text{Mg}_{1-x}\text{Al}_2\text{O}_4$). The study demonstrates a good agreement between anticipated band-gap values and experimental results, demonstrating the semiempirical model's usefulness. The large range of band-gap values reported in the literature for these spinels is explained by factors such as production methods, grain size, crystallographic defects, and impurities. These findings support the use of this semiempirical technique in band-gap engineering, allowing for the development of novel materials with tailored optical properties for a variety of applications.

Chapter 3: Experimentation

3.1. Materials

Cobalt acetylacetonate $\text{Co}(\text{acac})_2$ (97%), Gallium acetylacetonate $\text{Ga}(\text{acac})_3$, (99.99%), Nickel acetylacetonate $\text{Ni}(\text{acac})_2$, (95%), Nickel foam, Nafion, and ethanol were purchased from Sigma Aldrich and without any further treatment they were used.

3.2. Apparatus and Glassware

- Weighing balance
- Mortar and pestle.
- Glass dropper
- Tube furnace
- Ceramic boats
- Eppendorfs
- Pipette

3.3. Synthesis of CoGa_2O_4

To synthesize pristine cobalt gallium oxide (CoGa_2O_4), 1 mmol of $\text{Co}(\text{acac})_2$ and 2 mmol of $\text{Ga}(\text{acac})_3$ were combined with a few drops of ethanol (less than 0.5 mL). The mixture was grinded thoroughly using a mortar and pestle for approximately 5 min until it became homogeneous.

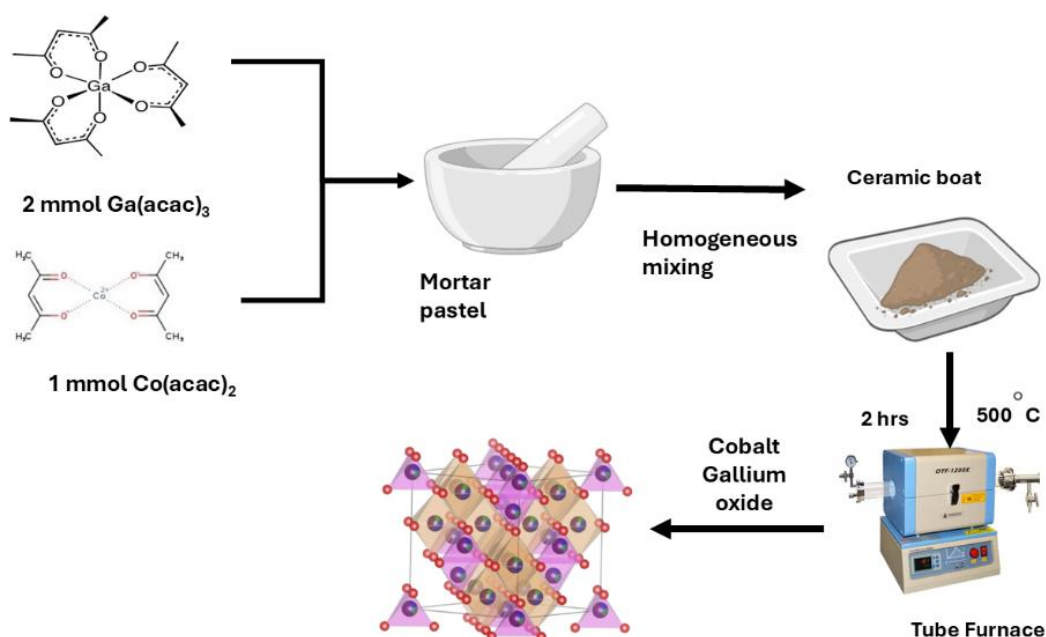


Figure 2. Schematic diagram for the synthesis of CoGa_2O_4 .

3.4. Synthesis of NiGa₂O₄

To synthesize pristine nickel gallium oxide (NiGa₂O₄), 1 mmol of Ni(acac)₂ and 2 mmol of Ga(acac)₃ were combined with a few drops of ethanol (less than 0.5 mL). The mixture was grinded thoroughly using mortar and pestle for approximately 5 minutes until it became homogeneous. The homogenized slurry was subsequently moved to a ceramic boat and placed in the center of the tube furnace. It was further heated to 500 °C for two hours under inert circumstances with N₂ gas. After cooling the furnace to room temperature, the product that emerged was collected for characterization. This sample is designated as NG.

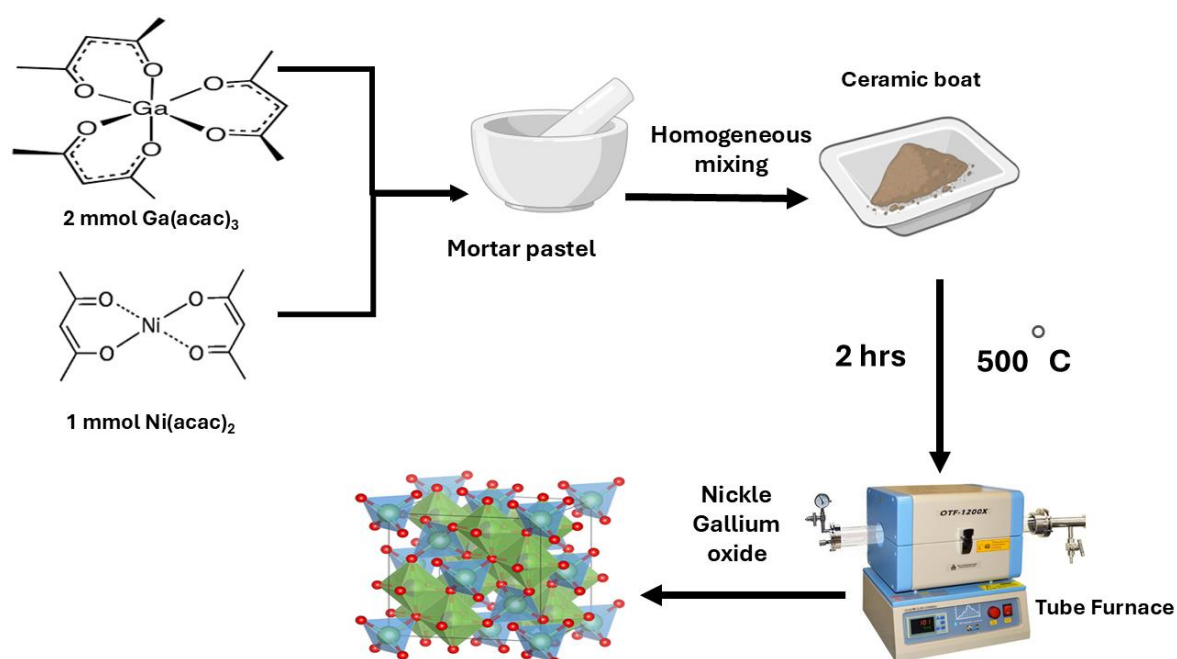


Figure 3. Schematic diagram for the synthesis of NiGa₂O₄

3.5. Synthesis of Co_xNi_{1-x}Ga₂O₄

To synthesize pristine cobalt gallium oxide (Co_xNi_{1-x}Ga₂O₄), x mmol of Ni(acac)₂, 1-x mmol of Co(acac)₂ and 2 mmol of Ga(acac)₃ were combined with a few drops of ethanol (less than 0.5 mL). The mixture was grinded thoroughly using mortar and pestle for approximately 5 min until it became homogeneous. The homogenized slurry was subsequently moved to a ceramic boat and placed in the center of the tube furnace. It was further heated to 500 °C for two hours under inert circumstances with N₂ gas. After cooling the furnace to room temperature, the product that emerged was collected for characterization.

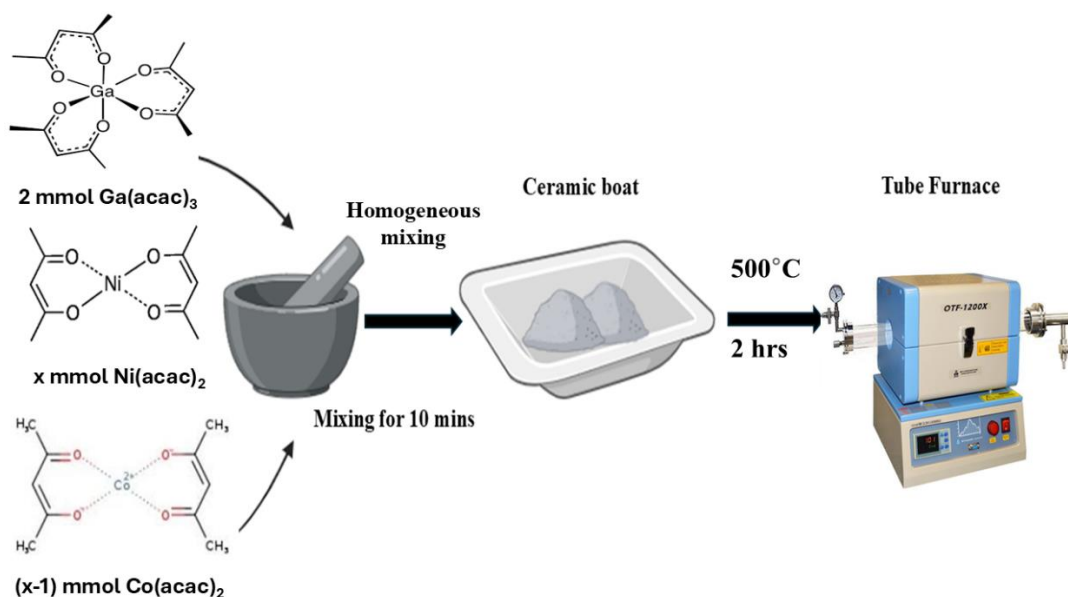


Figure 4. Schematic diagram for the synthesis of $\text{Co}_x\text{Ni}_{1-x}\text{Ga}_2\text{O}_4$

Table 2. Stoichiometric names of as-prepared samples.

Composite name	Label
CoGa_2O_4	CG
$\text{Co}_{0.8}\text{Ni}_{0.2}\text{Ga}_2\text{O}_4$	CNG-1
$\text{Co}_{0.6}\text{Ni}_{0.4}\text{Ga}_2\text{O}_4$	CNG-2
$\text{Co}_{0.4}\text{Ni}_{0.6}\text{Ga}_2\text{O}_4$	CNG-3
$\text{Co}_{0.2}\text{Ni}_{0.8}\text{Ga}_2\text{O}_4$	CNG-4
$\text{Co}_{0.5}\text{Ni}_{0.5}\text{Ga}_2\text{O}_4$	CNG-5
NiGa_2O_4	NG

3.6. Fabrication of electrode:

- **Activation of Nickel Foam (NF):** The nickel foam (NF) with dimensions of $1 \times 1 \text{ cm}^2$ is used as the substrate for the catalyst. To ensure the surface is free from any impurities or unwanted oxide layers, the nickel foam is cleaned multiple times. This cleaning process includes washing with hydrochloric acid (HCl) to remove any metal oxide, followed by rinsing with deionized water to remove any residual acid and then ethanol to further clean and remove any organic contaminants.[45]
- **Preparation of Catalyst Ink:** Once the NF substrate is cleaned, the next step involves preparing a catalyst ink. The ink is made by mixing the catalyst (a solid material) with Nafion, which is a proton-conductive polymer that helps bind the catalyst to the substrate

and ensures good electrical conductivity. In this case, 20 μL of Nafion is mixed with 3 mg of the catalyst. To make the mixture uniform and homogeneous, ethanol is added as a solvent. The ethanol helps dissolve and disperse the catalyst and Nafion uniformly, ensuring that the ink has the right consistency for application onto the nickel foam.

- **Drop-Casting Method:** Once the ink is prepared, it is applied to the cleaned nickel foam substrate using a drop-casting technique. In this method, the catalyst ink is carefully dropped onto the surface of the nickel foam ($1 \times 1 \text{ cm}^2$ area). The ink spreads across the foam, covering the surface where the catalyst particles will adhere. After the ink is applied, the sample is allowed to dry, typically at room temperature or in a mild heat setting, to ensure that the ink is fully evaporated, and the catalyst is securely bound to the nickel foam.
- **Electrochemical Testing:** After the catalyst is applied and dried, the modified nickel foam is ready for electrochemical testing. The electrochemical experiments are carried out directly on this modified nickel foam, which serves as both the substrate (supporting material) and the current collector (to provide electrical connection during testing). The electrochemical properties of the catalyst are typically tested in applications like water splitting (e.g., Oxygen Evolution Reaction or Hydrogen Evolution Reaction) to assess its performance.

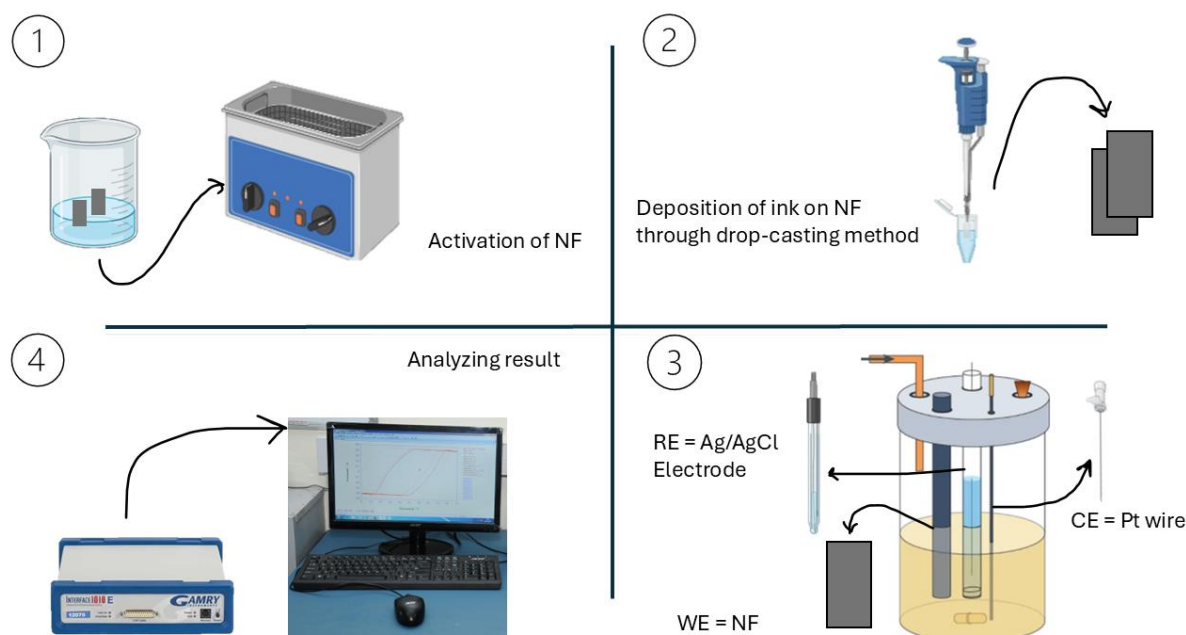


Figure 5. Schematic diagram for the fabrication of electrodes

Chapter 4: Results and Discussion

4.1. X-ray Diffraction Analysis

X-ray Diffraction (XRD) is a popular analytical technique that uses the contact of X-rays with materials to investigate the structural features of crystalline materials. This method is fundamental in materials science, chemistry, physics, geology, and other disciplines, allowing researchers to assess a material's crystalline structure, phase structure, and other structural properties. XRD relies on Bragg's Law, which explains the constructive interference of X-rays dispersed by atomic planes inside a crystal lattice. When an X-ray beam impacts a crystal, the atoms behave as scattering centers. Constructive interference arises when the difference in route length among rays scattered by neighboring planes is a multiple of the integer of the wavelength:

$$n\lambda=2d\sin\theta \quad (10)$$

where, n is Order of reflection (usually 1 for most practical purposes), λ is Wavelength of the applied X-ray beam, d is Interplanar spacing of the crystal lattice, and θ is Angle of incidence.

4.1.1. XRD Analysis

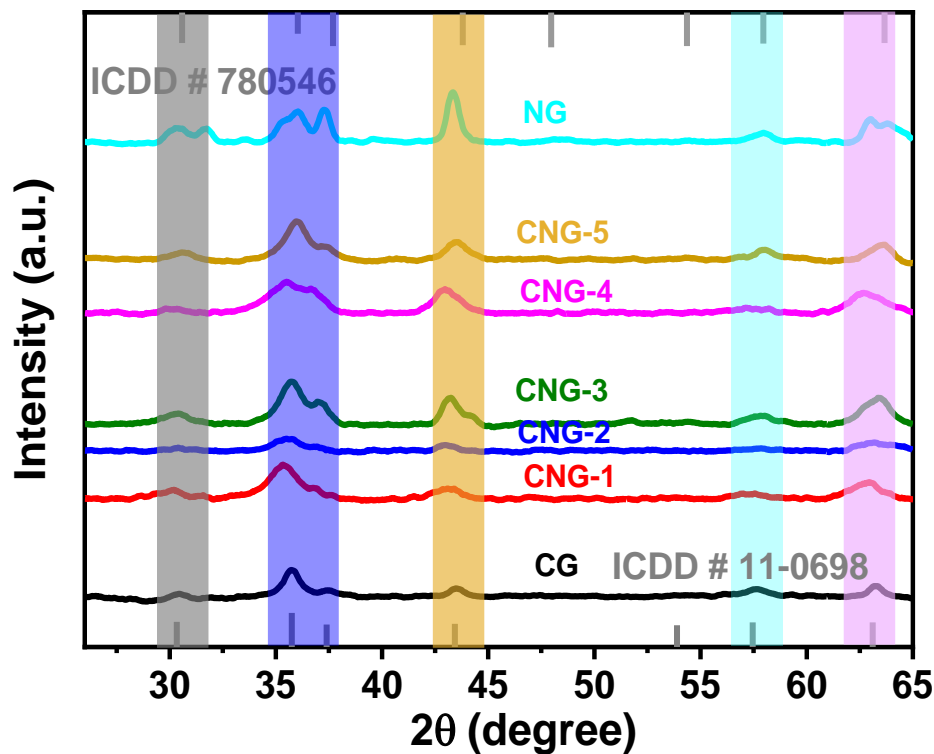


Figure 6. XRD spectra of CG, CNG-1, CNG-2, CNG-3, CNG-4, CNG-5, and NG

The provided XRD pattern shows the results of various samples identified as NG, CNG-5, CNG-4, CNG-3, CNG-2, and CNG-1, with reference to two ICDD files (780546 and #11-0698). The XRD peaks of the samples (CNG-1 to CNG-5 and NG) correspond to spinel phases, as suggested by the alignment with ICDD #780546 and #11-0698. The patterns are similar across the samples but exhibit slight variations in peak intensities and possibly minor shifts in peak positions. This suggests compositional or structural differences among the samples. The ICDD #780546 likely represents a CoGa_2O_4 spinel phase, as the pattern matches some of the Co-dominant samples. whereas ICDD #11-0698 corresponds to NiGa_2O_4 spinel. Peaks aligned with this reference appear in the NG (NiGa_2O_4) sample. The gradual shift in peaks from CNG-1 to CNG-5 indicates a progressive substitution of cobalt (Co) with nickel (Ni) in the spinel structure. This is expected since nickel and cobalt have slightly different ionic radii and electronic configurations, affecting the lattice parameters. The sharp and well-defined peaks across all samples indicate high crystallinity of the synthesized materials. Peak intensities vary between samples, which could reflect differences in relative crystallite size, sample texture, or preferential orientation during synthesis.

4.1.1.1. Interpretation of Specific Samples

1. **NG:** Matches closely with the ICDD #11-0698 pattern. Indicates a phase dominated by Ni substitution with negligible Co content.
2. **CNG-1 to CNG-5:** Represent Co-Ni-Ga mixed spinel phases. The progression from CNG-1 to CNG-5 likely represents a series with increasing Ni content and decreasing Co content.
3. **CNG-1:** Peaks align more closely with ICDD #780546, indicating a dominant CoGa_2O_4 phase.
4. **CNG-3 and CNG-4:** These samples show intermediate peak positions and intensities, reflecting a mixed Co-Ni phase with balanced substitution.
5. **CNG-5:** Peaks begin to align more with ICDD #11-0698, indicating a stronger presence of NiGa_2O_4 .

4.2. Fourier Transform Infrared Spectroscopy

Fourier Transform Infrared Spectroscopy (FTIR) is a potent analytical technique for identifying and analyzing materials using infrared absorption spectra. It is commonly used in chemistry, the study of materials, biological sciences, and environmental research to investigate the molecular layout, functional groups, and relationships of a sample. FTIR operates on the idea

that molecules collect infrared (IR) light at certain frequencies that correspond to the oscillations of their chemical bonds. When IR light penetrates a sample, specific frequencies are absorbed, resulting in a spectrum of absorption that acts as a "fingerprint" for the substance. The vibrations include stretching- the elongation or compression of bonds, and bending- changes in bond angles (scissoring, rocking, wagging, or twisting). The relationship between the absorbed energy and bond vibrations is described by the equation:

$$E = h\nu \quad (11)$$

Where, E is the energy of vibration, h refers to Planck's constant, and ν is the frequency of the vibration

4.2.1. FTIR Analysis

The provided FTIR spectra shows the vibrational features of samples NG, CNG-5, CNG-4, CNG-3, CNG-2, and CNG-1.

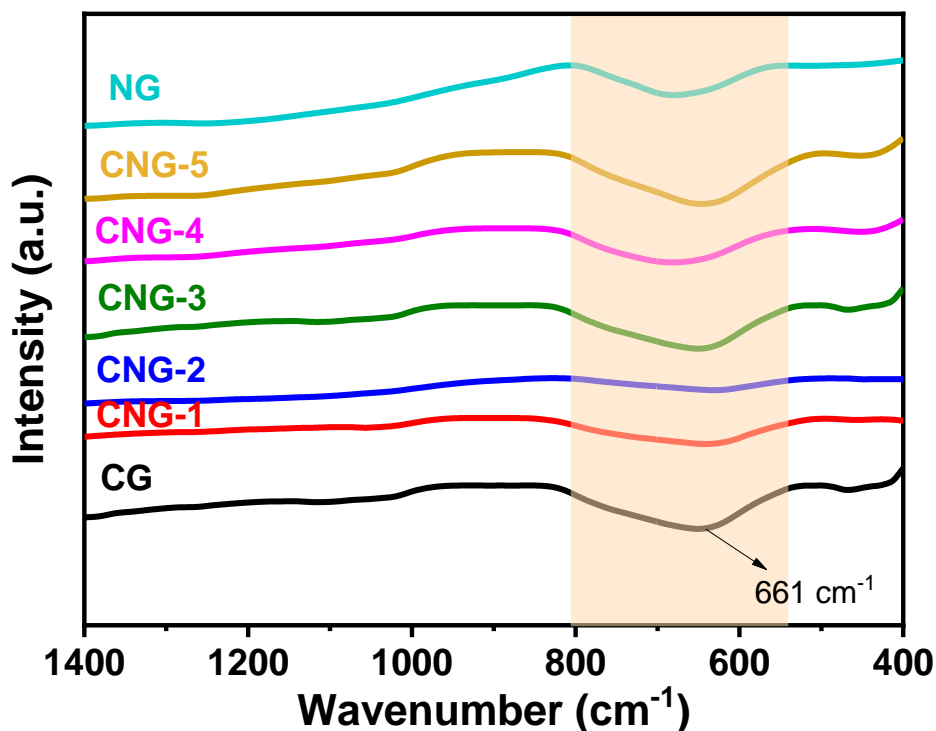


Figure 7. FTIR spectra of CG, CNG-1, CNG-2, CNG-3, CNG-4, CNG-5, and NG.

4.2.1.1. Key Observations

1. The highlighted region in the spectra, near **66 cm⁻¹**, corresponds to specific vibrational modes of the material. These could indicate stretching or bending vibrations of metal-oxygen bonds, which are typical for spinel structures like CoNiGa₂O₄ or NiGa₂O₄.
2. The shift in peak position across samples suggests systematic changes in the chemical environment due to compositional variation (e.g., the gradual substitution of Co with Ni).
3. For spinel oxides, FTIR peaks typically appear in two regions:
 - **400–600 cm⁻¹**: Corresponds to M-O stretching vibrations in tetrahedral and octahedral sites, M = Co, Ni, Ga in this case
 - The slight shifts in these vibrations indicate changes in lattice dynamics due to the varying Co/Ni ratios.
4. The intensities of the peaks vary slightly among the samples, suggesting differences in crystallinity or sample composition. Higher peak intensities often correlate with better crystalline order, while broader peaks could indicate amorphous or poor crystalline structures.
5. As Co is gradually replaced by Ni, the peak shifts may reflect changes in bond strength. For instance:
 - Ni²⁺ has a slightly smaller ionic radius than Co²⁺, which could lead to stronger bonds and higher vibrational frequencies.
 - The observed shift could also result from altered cation distribution between tetrahedral and octahedral sites.
6. The systematic changes in the FTIR spectra confirm that all samples belong to a spinel structure but exhibit subtle variations in local bonding environments due to the different Co/Ni compositions.

4.3. Scanning electron Microscopy

Scanning Electron Microscopy (SEM) is a popular investigative technique for imaging and analyzing materials' surface properties and composition. SEM delivers excellent quality three-dimensional images as well as comprehensive data on a sample's topography, anatomy, and composition. SEM works by scanning a concentrated stream of electrons over the outermost

layer of a sample. The interaction between the electron beam and the sample produces a variety of indications, notably secondary electrons, backscattered electrons, and distinctive X-rays. These signals are gathered and processed to provide pictures or compositional data.

4.3.1. SEM Analysis

The provided SEM images showcase the surface morphology of seven distinct samples labeled (a) to (g).

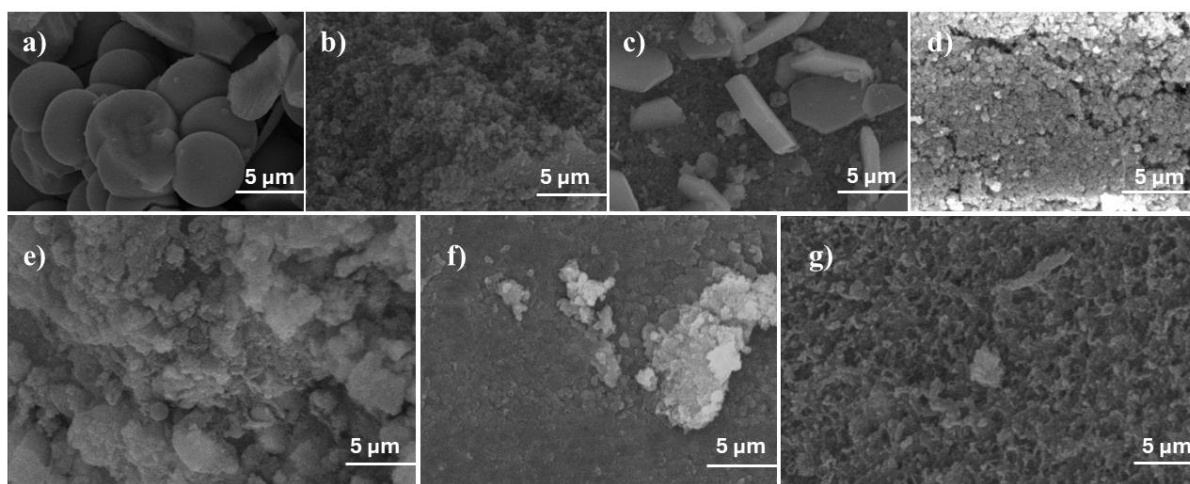


Figure 8. Scanning electron microscopy (SEM) images of a) CG, b) CNG-1, c) CNG-2, d) CNG-3, e) CNG-4, f) CNG-5, and g) NG at a resolution of 5 μm.

4.3.1.1. Key Observations

(a) CG

- **Structure:** Large, disk-like platelets with smooth surfaces, indicative of a well-defined crystalline morphology.
- **Interpretation:** This structure might suggest high crystallinity or a specific growth mechanism leading to uniform flat particles.
- **Potential Use:** Such morphology can influence the material's active surface area and catalytic performance.

(b) CNG-1

- **Structure:** Amorphous-like or highly porous clusters with undefined shapes.
- **Interpretation:** Indicates a less crystalline structure or a material with higher porosity, likely enhancing surface activity in catalytic processes.

(c) CNG-2

- **Structure:** Sharp-edged particles, possibly rod- or shard-like shape, arranged randomly.
- **Interpretation:** These features may arise from anisotropic crystal growth, leading to elongated structures. The sharpness of edges could improve catalytic activity.

(d) **CNG-3**

- **Structure:** Fine, dense granular morphology with no significant porosity or voids visible.
- **Interpretation:** Compact nature suggests high packing density, which could affect surface area and electrochemical performance.

(e) **CNG-4**

- **Structure:** Aggregated, flake-like particles forming dense clusters.
- **Interpretation:** The flake morphology suggests layered growth, which may offer higher interfacial interaction with electrolytes in catalytic applications.

(f) **CNG-5**

- **Structure:** Irregularly shaped particles interspersed with some larger fragments or aggregates.
- **Interpretation:** These inconsistencies might indicate uneven nucleation or growth during synthesis, leading to heterogeneous structures.

(g) **NG**

- **Structure:** A highly porous network with interconnected voids.
- **Interpretation:** Such a porous structure is beneficial for applications requiring high surface areas, such as catalysis or energy storage.

The SEM images reveal a diverse range of morphologies, from well-defined platelets (a) to highly porous structures (g).

4.4. Energy Dispersive Spectroscopy

Energy Dispersive X-Ray Spectroscopy, additionally referred to as Energy Dispersive X-Ray Analysis (EDXA), is an investigative technique used to identify elements and quantitatively analyze materials. It is often used in conjunction with Scanning Electron Microscopy or

Transmission Electron Microscopy to deliver compositional data on microscopic portions of a sample.

4.4.1. EDS Analysis

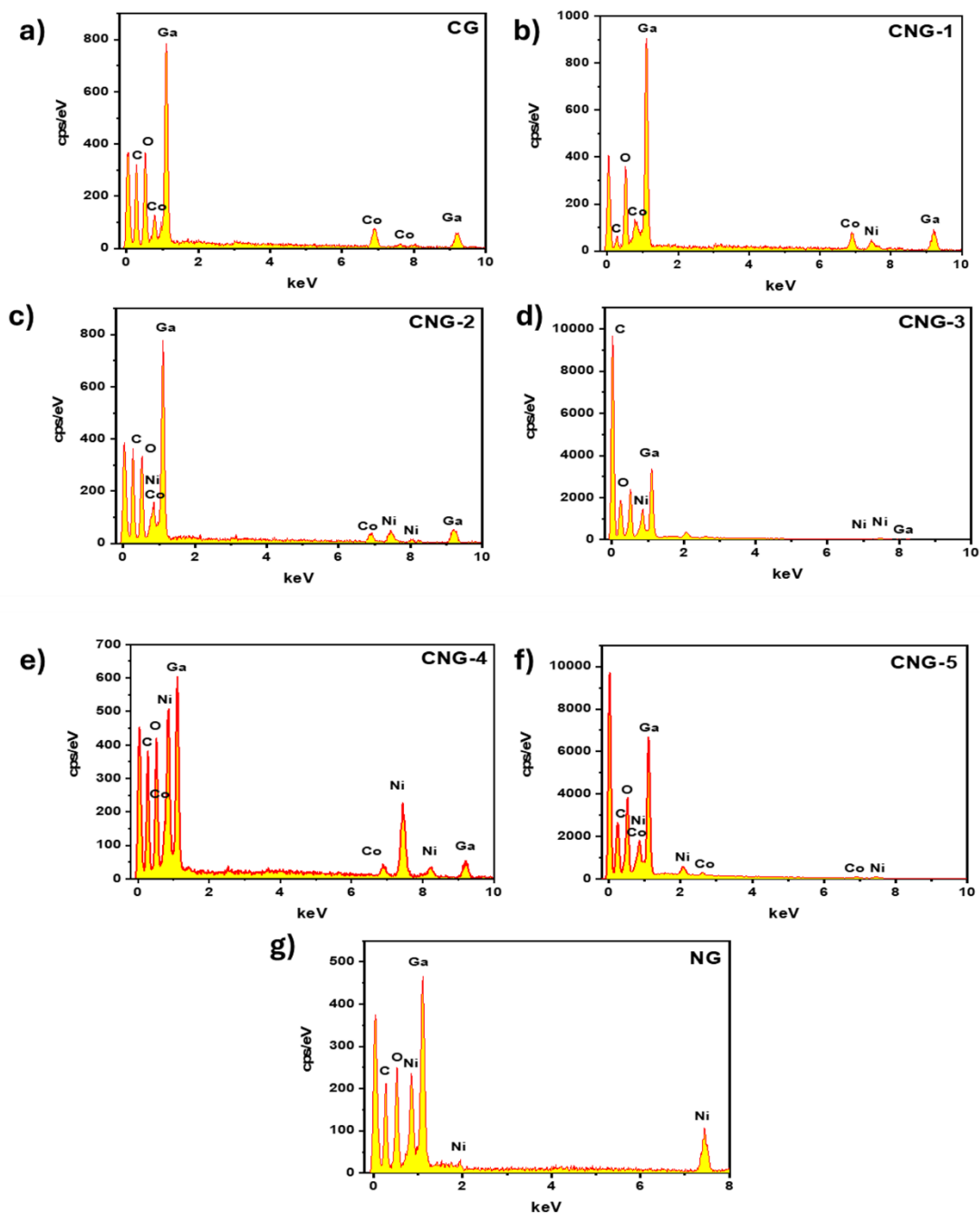


Figure 9. EDX spectra of a) CG, b) CNG-1, c) CNG-2, d) CNG-3, e) CNG-4, f) CNG-5, and g) NG.

An EDS analysis of synthesized CoGa_2O_4 , NiGa_2O_4 , and $\text{CoNiGa}_2\text{O}_4$ particles identified characteristic peaks for Gallium at $K\alpha$ (1.2 keV) and $K\beta$ (around 9.12 keV) and Cobalt at $K\alpha$

(around 0.87 keV). These peaks in figure 13 confirm the chemical purity and elemental composition of the $\text{CoNiGa}_2\text{O}_4$ material.

4.5. Transmission Electron Microscopy

Transmission Electron Microscopy is a sophisticated analytical technique that visualizes the interior framework of materials at molecular and nanoscale resolutions. TEM is used extensively in the fields of material science, biology, nanotechnology, and other domains to study crystallography, morphology, and composition. TEM works by sending a high-energy electron beam (usually 80-300 keV) through an ultrathin material. Electrons react with the sample and are dispersed, absorbed, or transmitted based on the density and composition of the material. The electrons that are transmitted are collected to produce highly detailed pictures or diffraction patterns, which disclose details about the sample's interior structure.

4.5.1. TEM Analysis

This image presents high-resolution transmission electron microscopy analysis, showing structural and lattice details of a material.

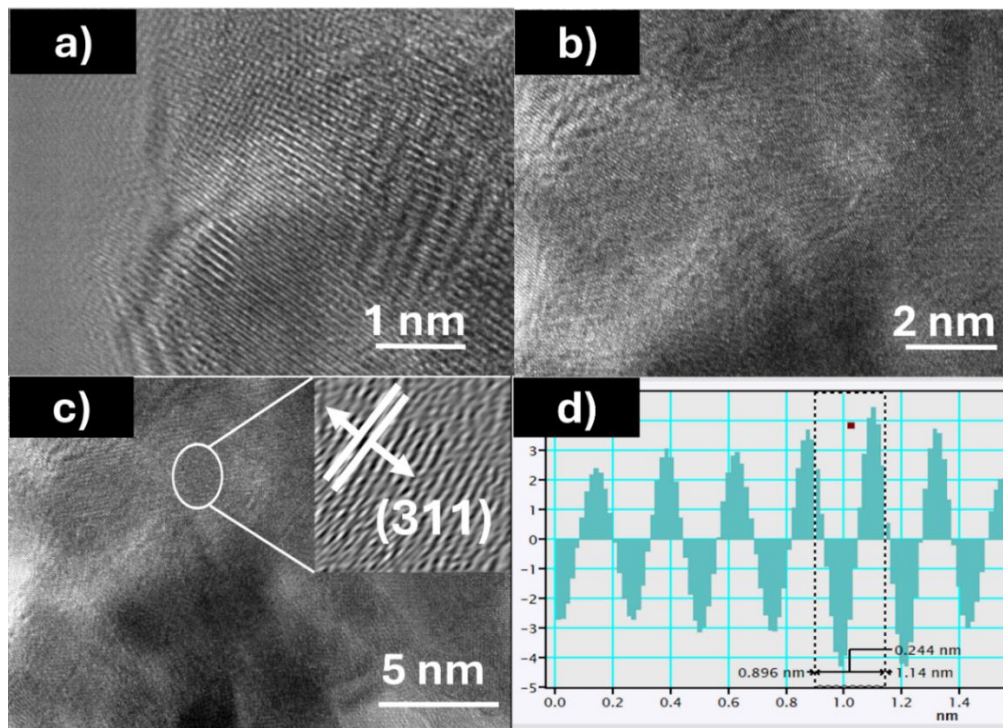


Figure 10. Transmission Electron Microscopy images of CNG-5 at a) 1nm, b) 2nm, c) 5nm with an inset showing IFFT image, and d) live profile image showing interplanar d spacing.

4.5.1.1. Key Observations

1. Shows well-defined lattice fringes, indicating a crystalline structure.

2. The periodic pattern of fringes suggests a specific crystallographic orientation.
3. Spacing between the fringes can be measured to determine interplanar spacing (d-spacing) corresponding to specific planes in the crystal lattice.
4. All images show strong evidence of crystalline domains.
5. The observed lattice fringes and d-spacing values suggest high-quality crystallinity with specific planes visible (e.g., (311)).
6. The presence of clear fringes with consistent spacing indicates that the material is structurally ordered.
7. Variations in intensity or defects visible in (b) and (c) could indicate grain boundaries, stacking faults, or other imperfections.
8. The (311) plane and measured d-spacing can be compared to reference values from databases (e.g., JCPDS) to identify the material and its phase.

4.6. Differential Scanning Calorimetry

DSC is a scientific technique that investigates the thermal behavior of materials. It quantifies the heat flow caused by phase transitions, chemical processes, or other thermal processes because of temperature or time. DSC is commonly used in material science, polymers, medications, and the food industry to characterize features such as melting points, crystallization, and heat stability. DSC works by detecting the differential in heat flow among the specimens and a reference material while they undergo exposure to a regulated temperature program.

4.6.1. DSC analysis

This image shows a Differential Scanning Calorimetry curve for the sample labeled CNG-4, plotting heat flow (mV) against sample temperature (°C).

4.6.1. Key Observations

- 1) The curve slopes downward as the temperature increases, indicating an endothermic process where heat is absorbed by the sample.
- 2) This could correspond to phase transitions, decomposition, or other thermal events.
- 3) Significant changes occur primarily between 200°C and 500°C.
- 4) There appears to be a notable feature around 300–350°C, as highlighted in the inset, likely indicating a thermal event (e.g., phase transition, melting, or a chemical reaction).
- 5) The inset zooms into the 200–400°C range, providing more detail on the thermal event around 300–350°C.

- 6) This region might correspond to a specific structural or chemical change, such as:
 - i) Decomposition of a phase.
 - ii) Crystallization or melting of a component.
- 7) The gradual slope suggests continuous thermal processes like phase changes or gradual weight loss (e.g., evaporation or decomposition of volatile species).
- 8) The event at 300–350°C might represent a solid-state phase transition or recrystallization process.
- 9) If the material is metallic or alloy-based (as suggested by earlier TEM and EDS results), this could involve lattice rearrangement or oxidation.
- 10) The heat absorption over a wide range of temperatures may indicate decomposition of an organic or other thermally unstable component.
- 11) If CNG-4 contains components with melting points in this range, the observed feature could correspond to melting or crystallization.

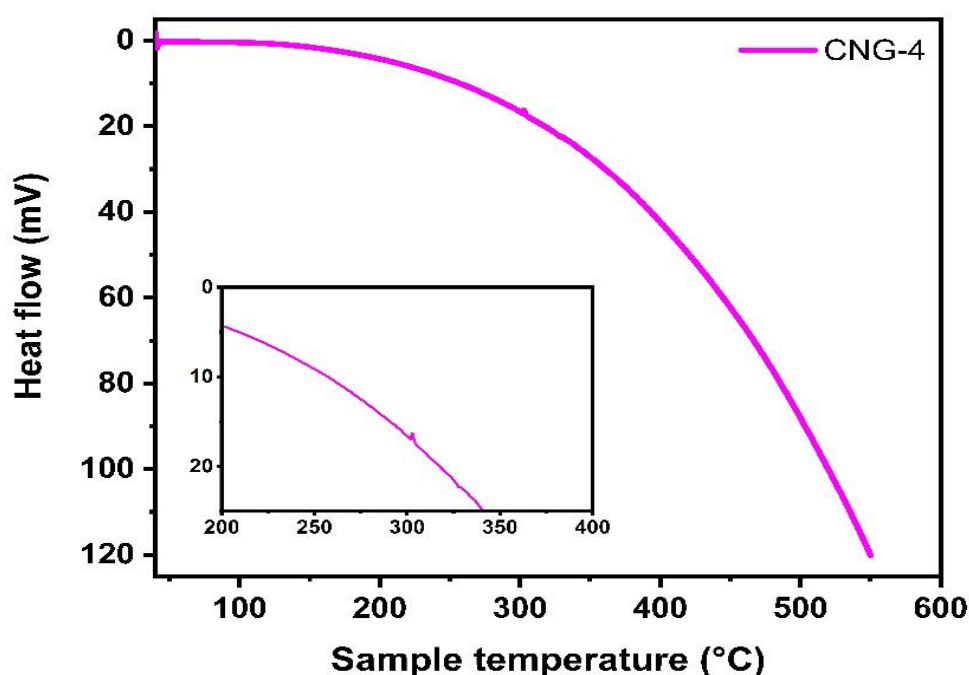


Figure 11. DSC analysis of CNG-4.

4.7. Electrochemical Analysis

Electrochemical investigations were carried out using a Gamry Interface 1000E Potentiostat (734 Louis Drive, Warminster, PA 18974, USA) with a conventional three-electrode configuration. The electrochemical performance of the produced samples was evaluated

utilizing techniques including Cyclic Voltammetry, Linear Sweep Voltammetry, Electrochemical Surface Area measurement, Electrochemical Impedance Spectroscopy, and Chronoamperometry. The electrolytes for oxygen evolution reaction and hydrogen evolution reaction investigations were 1 M KOH (pH = 13.0) and 0.5 M H₂SO₄ (pH = 1.0), respectively. The OER setup consisted of three electrodes: the prepared electrodes as operating electrodes, an Ag/AgCl electrode as standard electrode, and a platinum wire as opposing electrode. To convert potential measured against Ag/AgCl to the reversible hydrogen electrode (RHE) scale, the Nernst equation was applied:

$$E_{\text{RHE}} = E_{\text{Ag/AgCl}} + 0.197 + 0.059 \times \text{pH} \quad (12)$$

In this equation, $E_{\text{Ag/AgCl}}$ denotes the experimentally determined potential against the Ag/AgCl reference, and E_{RHE} denotes the comparable potential versus RHE. The phrase 0.197 V refers to the Ag/AgCl reference electrode's conventional thermodynamic potential. To prepare for electrochemical evaluations, the working electrodes were conditioned prior to use with CV at an increased scan rate of 100 mV s⁻¹. This technique stabilized the electrodes and set them up for reliable operation in future experiments. LSV was done at a slower scan rate of 5 mV/s to estimate the onset overpotential, which is the additional potential needed to commence water oxidation above the thermodynamic potential of 1.23 V versus RHE [46, 47]. The overpotential (η) was determined with the following equation:

$$\eta = E_{\text{RHE}} - 1.23 \text{ V} \quad (13)$$

Tafel analysis was conducted to understand the charge transfer kinetics and analyze the rate-determining step. The Tafel slope was obtained from the following equation:

$$\eta = a + b \cdot \log(j) \quad (14)$$

Here, η is the overpotential, a is the Tafel constant, j is the current density normalized by the geometric area, and b is the Tafel slope. The Tafel slope (b) is derived from $b = 2.303 RT/nF$, where R is the universal gas constant, T is the absolute temperature, n is the number of electrons involved in the reaction, and F is Faraday's constant. The Tafel slope provides crucial insights into the kinetics of electrochemical reactions. A lower slope indicates faster charge transfer and enhanced-catalytic efficiency. These measures collectively help evaluate the efficiency, stability, and activity of the catalysts under study, providing detailed insights into their performance in OER and HER.[48-50]

4.8. Oxygen Evolution Reaction

The image displays Linear Sweep Voltammetry curves and corresponding overpotential bar graphs for different catalysts under evaluation for their electrocatalytic performance. LSV plots depicts the effect of current density (mA/cm²) on y-axis and potential (V vs. RHE) on x-axis. The catalyst labeled CNG-4 demonstrates the highest current density at a given potential, indicating superior electrocatalytic activity compared to other catalysts. The onset potential (the point where current density begins to rise significantly) appears to be lowest for CNG-4, suggesting that this catalyst has the lowest activation energy for the electrochemical reaction. The performance hierarchy based on current density can be summarized as:

$$\text{CNG-4} > \text{CNG-3} > \text{CNG-5} > \text{CG} > \text{CNG-2} > \text{CNG-1} > \text{NG}.$$

NG shows the poorest performance, with significantly lower current density and a delayed onset potential. Overpotential (η) is the extra potential needed outside the thermodynamic equilibrium potential to run the electrochemical reaction at a specific current density (50 mA/cm²). Lower overpotential reflects higher catalytic efficiency. CNG-4 exhibits the lowest overpotential of 300 mV, confirming its high efficiency. The overpotential ranking is consistent with the LSV results:

$$\text{CNG-4 (300 mV)} < \text{CNG-3 (339 mV)} < \text{CNG-5 (348.3 mV)} < \text{CG (355.8 mV)} < \text{CNG-2 (367.7 mV)} < \text{CNG-1 (396 mV)} < \text{NG (540.7 mV)}.$$

The significantly higher overpotential for NG (540.7 mV) suggests that this material is not suitable as an electrocatalyst in its current form. The relatively close overpotential values of CNG-4, CNG-3, and CNG-5 indicate that these catalysts are promising candidates, with CNG-4 being the most efficient. CNG-4 outperforms all other catalysts for current density and overpotential, making it the most promising candidate for the electrochemical reaction under study (likely oxygen evolution reaction (OER) or hydrogen evolution reaction (HER)). The results suggest that the modifications or composition of CNG-4 optimize the active sites, electronic properties, or surface area, leading to enhanced catalytic activity.

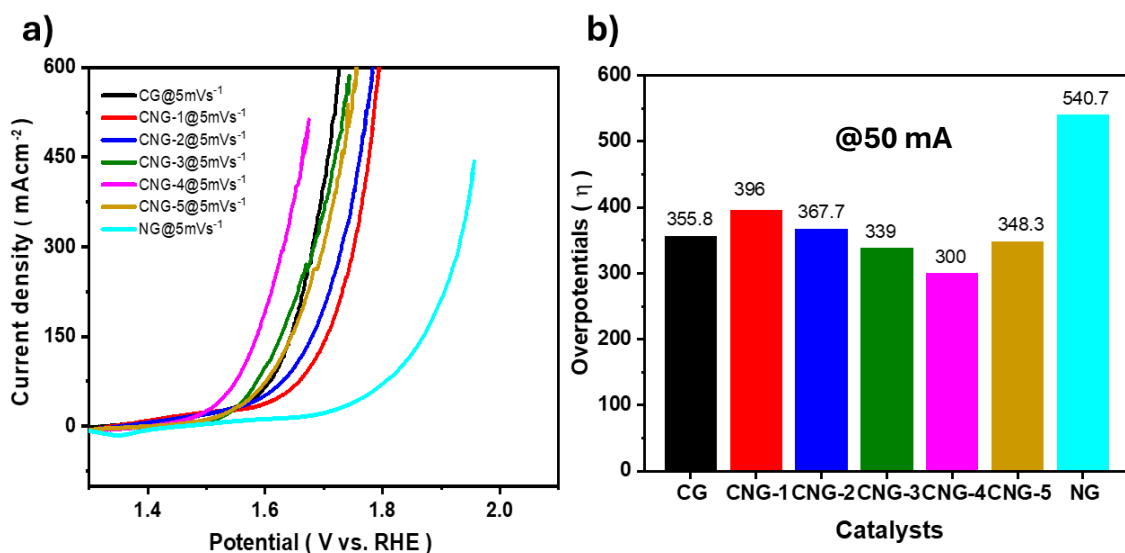


Figure 12. a) Linear Sweep Voltammetry (LSV) curves, and b) bar graph showing overpotential values of CG, CNG-1, CNG-2, CNG-3, CNG-4, CNG-5, and NG at 50 mA with a scan rate of 5 mV s⁻¹ in 1 M KOH

The figure 19 a) displays the Tafel slopes for various catalysts, which provide insight into their electrochemical kinetics for oxygen evolution reaction (OER) The Tafel slope (b) is obtained from the Tafel equation:

$$\eta = b \cdot \log(j) + a \quad (15)$$

where η is the overpotential, j is the current density, and bb reflects the kinetic rate of the reaction. A smaller Tafel slope indicates faster kinetics and more efficient charge transfer processes.

Table 3. The catalysts show varying Tafel slopes.

Composites	Tafel slope value (mV dec ⁻¹)
CG	126.7
CNG-1	226.4
CNG-2	183.7
CNG-3	127.1
CNG-4	96.42
CNG-5	120.36
NG	194.22

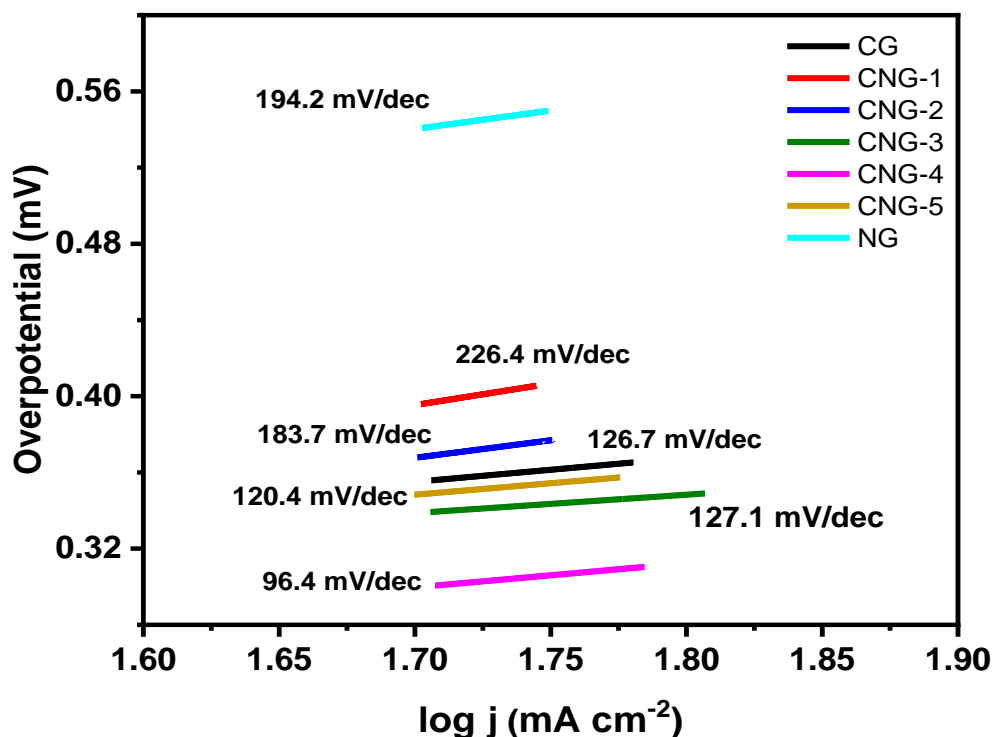


Figure 13. Tafel slope values of CG, CNG-1, CNG-2, CNG-3, CNG-4, CNG-5, and NG at current density of 50 mA.

CNG-4 exhibits the smallest Tafel slope (96.42 mV/dec), indicating the fastest reaction kinetics and the most efficient catalytic activity among the catalysts tested. CNG-2, CNG-3, and CG show moderate Tafel slopes (~126.77 mV/dec), suggesting relatively efficient but slower kinetics compared to CNG-4. CNG-5 also demonstrates good kinetics with a Tafel slope of 120.36 mV/dec. NG and CNG-1 display the highest Tafel slopes (194.22 mV/dec and 226.42 mV/dec, respectively), suggesting sluggish reaction kinetics and poor catalytic performance. The Tafel slopes indicate that CNG-4 is likely to have an increased density of active sites, improved charge transfer efficiency, or a favorable reaction pathway, making it the most effective catalyst for the electrochemical process studied. The significantly higher Tafel slopes for NG and CNG-1 suggest that these catalysts either lack sufficient active sites or have intrinsic limitations in their material properties. CNG-4 stands out as the most kinetically efficient catalyst, with the smallest Tafel slope, making it a promising candidate for the targeted electrochemical reaction. NG and CNG-1 are the least efficient, indicating the need for material modification or optimization. Further studies, such as stability tests or computational modeling, could validate the observed trends and provide deeper insights into the reaction mechanisms for these catalysts.

4.8.1. Electrochemically Active Surface Area

Figure 21 shows the double-layer capacitance (C_{dl}) numbers, which are used to calculate the electrochemical active surface area of different catalysts. The double-layer capacitance (C_{dl}) correlates to the electrochemical active surface area, with a constant specific capacitance per unit area. C_{dl} is calculated as the slope of current density (j) vs. scan rate (v) in the non-faradaic zone.

$$ECSA = \frac{\text{Double layer capacitance (Cdl)}}{\text{Specific capacitance } C_s} \quad (16)$$

Table 4. C_{dl} values of different composites.

Composite name	ECSA (mF/cm ²)
CG	7.1
CNG-1	7.9
CNG-2	10.6
CNG-3	10.9
CNG-4	27.5
CNG-5	10.4
NG	7.1

CNG-4 has the highest C_{dl} (27.5 mF/cm²), indicating the largest ECSA and suggesting the highest density of electrochemically active sites among the tested catalysts. CNG-2, CNG-3, and CNG-5 exhibit moderate C_{dl} values (10.65–10.94 mF/cm²), indicating a reasonably high ECSA and good catalytic potential. CG, CNG-1, and NG show lower C_{dl} values (~7.11–7.9 mF/cm²), indicating smaller ECSAs and potentially fewer active sites. A higher C_{dl} corresponds to a larger ECSA, which improves the catalyst's interaction with the electrolyte, enabling more efficient charge transfer and reaction kinetics. The superior performance of CNG-4 aligns with its higher C_{dl} , supporting its role as the most active catalyst in this study. The linearity of the plots suggests a consistent and reliable determination of C_{dl} values. Catalysts with higher C_{dl} values are expected to exhibit better performance in electrochemical reactions (e.g., HER or OER), as observed in previous analyses. CNG-4 is the standout catalyst in terms of ECSA, as evidenced by its significantly higher C_{dl} value. This corresponds to a greater number of accessible active sites, enhancing their catalytic activity. CNG-2, CNG-3, and CNG-5 also exhibit good C_{dl} values, making them promising candidates for further

evaluation. The lower Cdl values for CG, CNG-1, and NG suggest the need for material modification or optimization to increase their active surface areas.

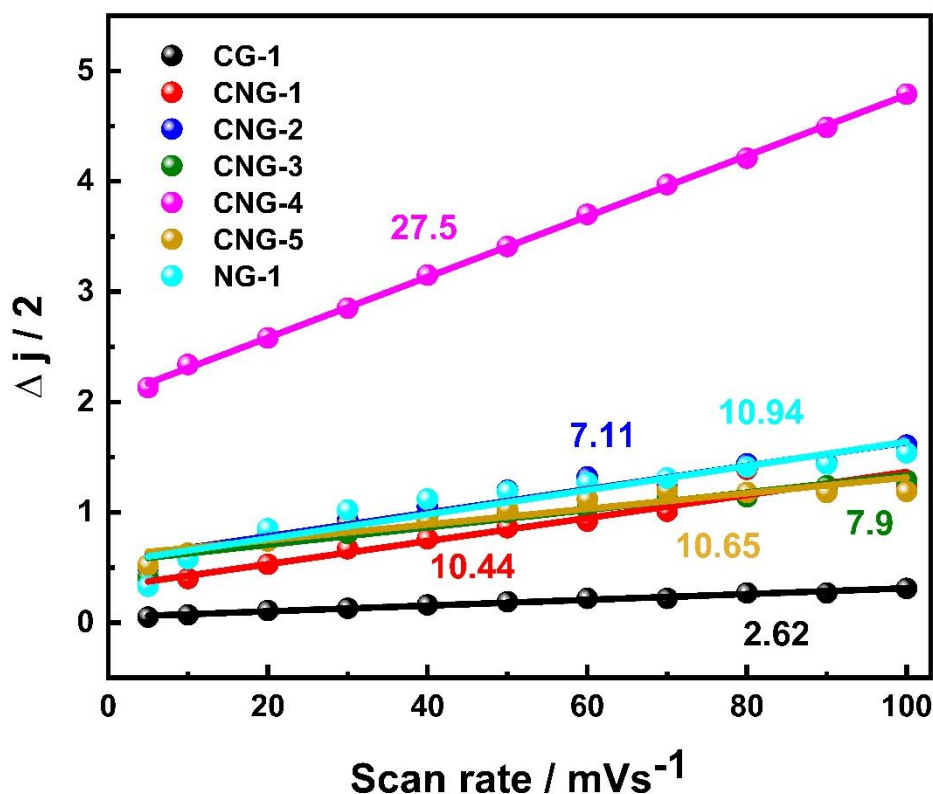


Figure 14. C_{dl} values of CG, CNG-1, CNG-2, CNG-3, CNG-4, CNG-5, and NG.

A lower Tafel slope is indicative of faster charge transfer kinetics during the catalytic reaction (e.g., HER or OER). CNG-4, with the highest Cdl (27.5 mF/cm²), also shows a favorable Tafel slope of 96.42 mV/dec, signifying highly efficient reaction kinetics. CNG-3, CNG-2, and CNG-5 exhibit moderate Cdl values (10.65–10.94 mF/cm²) and Tafel slopes between 120.36 and 126.77 mV/dec, indicating reasonably good kinetic activity. CG, CNG-1, and NG, with lower Cdl, have higher Tafel slopes (126.77–226.42 mV/dec), which correlates with reduced catalytic efficiency. Catalysts with higher Cdl (i.e., larger ECSA) generally exhibit lower Tafel slopes, affirming the role of active surface area in improving catalytic reaction kinetics. A lower overpotential at a fixed current density (e.g., 50 mA/cm²) reflects better catalytic efficiency. CNG-4, with the highest Cdl, achieves the lowest overpotential (300 mV), indicating that its high ECSA enhances reaction efficiency. CNG-2, CNG-3, and CNG-5, with moderate Cdl, exhibit overpotentials ranging from 339 mV to 348.3 mV, showing good but slightly lower catalytic efficiency compared to CNG-4. CG, CNG-1, and NG, with the

lowest Cdl, require significantly higher overpotentials (355.8–540.7 mV), further demonstrating the importance of active surface area in reducing energy barriers.

1. **CNG-4**: Best performer, combining the highest ECSA, the lowest Tafel slope, and the lowest overpotential.
2. **CNG-2, CNG-3, and CNG-5**: Moderate performance, with good ECSA values, reasonable Tafel slopes, and moderate overpotentials.
3. **CG, CNG-1, and NG**: Lower-performing catalysts, limited by smaller ECSA, higher Tafel slopes, and higher overpotentials.

The strong correlation between Cdl, Tafel slopes, and overpotentials highlights the critical role of ECSA in enhancing catalytic efficiency. CNG-4's superior performance can be attributed to its significantly larger ECSA, facilitating efficient charge transfer and reduced energy barriers. Future work could focus on modifying lower-performing catalysts (e.g., CG, NG) to increase their Cdl, such as by optimizing their morphology, porosity, or surface functionalization.

4.8.2. Electron Impedance Spectroscopy

Figure 22 shows Electrochemical Impedance Spectroscopy (EIS) data, presented as Nyquist plots a) and a bar chart b) with a circuit model diagram at the bottom c).

➤ Observation

1. The Nyquist plot displays the imaginary component of impedance ($-Z''$) versus the real component (Z').
2. The semicircles represent the charge transfer resistance (R_{ct}) for different catalysts, with labels such as CG, CNG-1, CNG-2, CNG-3, CNG-4, CNG-5, and NG.
3. Catalysts like CNG-4 and CNG-5 exhibit much smaller semicircles, indicating significantly lower R_{ct} , which correlates to better catalytic activity and higher charge transfer efficiency.
4. Conversely, CG and NG-1 show larger semicircles, indicating higher R_{ct} , implying slower charge transfer kinetics and poorer performance.
5. The inset magnifies the low-impedance region, clearly showing the hierarchy in R_{ct} , where CNG-4 performs the best, followed by CNG-5.

The bar chart quantifies R_{ct} values derived from the Nyquist plots. R_{ct} is smallest for CNG-4 (24.6 Ω) and CNG-5 (26 Ω), confirming their superior catalytic activity. NG-1 exhibits an extremely high R_{ct} of $6.79 \times 10^6 \Omega$, signifying very poor performance. CG and CNG-1 show intermediate R_{ct} values (232.5 Ω and 174.6 Ω , respectively). The trend clearly shows the evolution of performance across the catalyst series, likely due to modifications in composition or structure improving charge transfer. The circuit includes:

- **Ru**: Uncompensated resistance, representing the solution resistance.
- **Rp**: Charge transfer resistance (R_{ct}).
- **Y0 and α** : Represent a constant phase element (CPE), modeling non-ideal capacitive behavior.

This equivalent circuit is typically used to fit the Nyquist data to extract parameters such as R_{ct} , which are indicative of catalytic activity and electrode kinetics. Catalysts CNG-4 and CNG-5 demonstrate the best performance due to their minimal R_{ct} , suggesting high charge transfer efficiency and superior catalytic activity. The NG-1 catalyst has an exceptionally poor performance with an extremely high R_{ct} . The EIS data indicates the effectiveness of tuning the catalyst properties, where the CNG series outperforms CG and NG-1, likely due to enhancements in their surface structure, conductivity, or active site density.

Table 5. R_{ct} and R_s values of catalyst in 1M KOH.

Composite name	Solution resistance R_s (Ω)	Charge-transfer resistance R_{ct} (Ω)
CG	1.78	232.5
CNG-1	898.1×10^{-3}	174.6
CNG-2	1.71	76.8
CNG-3	2.39	62.9
CNG-4	1.25	24.6
CNG-5	1.57	26
NG	1.52	6.7×10^7

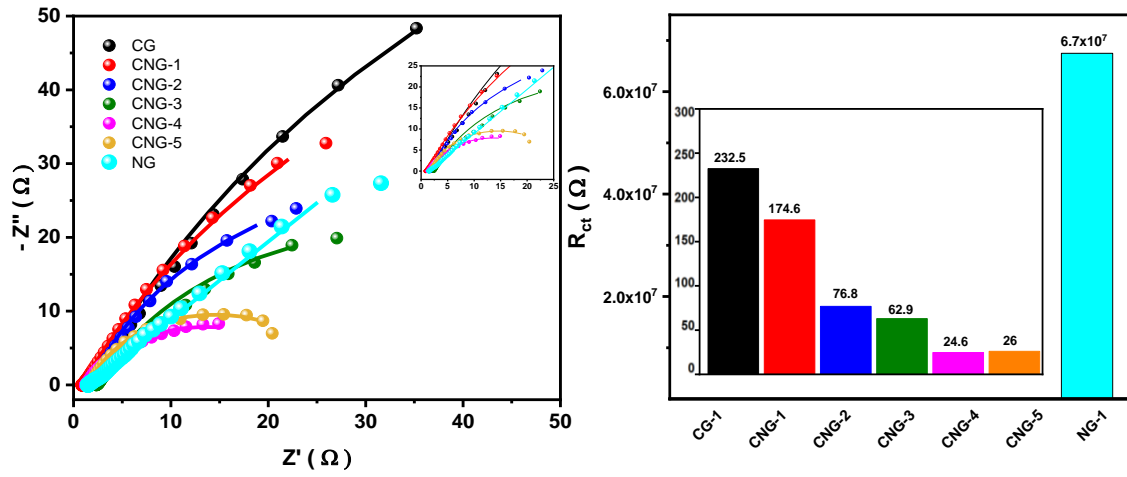


Figure 15. a) Nyquist plots, and b) bar graph showing R_{ct} values of CG, CNG-1, CNG-2, CNG-3, CNG-4, CNG-5, and NG.

Chapter 5: Conclusion

This study successfully synthesized a series of composites through a solventless method, demonstrating a sustainable and environmentally friendly approach to catalyst preparation. The solventless technique ensures minimal waste production and avoids the use of harmful organic solvents, aligning with the principles of green chemistry. Each catalyst in this series was systematically designed to investigate its structural, morphological, and electrochemical properties, focusing particularly on their participation in the oxygen evolution reaction. The catalysts have various structural and compositional features that influenced their catalytic behavior. Their crystal structures, validated by X-ray diffraction (XRD), and surface structures, detected by scanning electron microscopy (SEM), demonstrated the solventless synthesis method's efficacy in preserving homogeneity and intended phases throughout the series. Electrochemical activity evaluations demonstrated that all the catalysts exhibited significant OER activity under alkaline conditions. Cyclic voltammetry (CV) and linear sweep voltammetry (LSV) studies revealed variations in their overpotentials and current densities, highlighting the impact of composition and structure on catalytic performance. Tafel slope analysis further indicated the kinetic parameters, emphasizing differences in reaction pathways and the role of intrinsic catalytic properties. Notably, the catalyst containing 0.8 moles of Nickel and 0.2 mol of Cobalt showed extraordinary OER performance, achieving a low overpotential at a current density of 50 mA and a high turnover frequency (TOF). On the other hand, catalysts with 0.8 moles of Cobalt and 0.2 moles of Nickel demonstrated moderate activity, suggesting the potential for further optimization through compositional or structural modifications. The catalysts' stability was further tested using chronopotentiometry, for long-time cyclic tests, confirming their durability under extended electrochemical operations. The catalyst, CNG-4 exhibited the highest stability, retaining over 69% of its initial activity after prolonged testing. This demonstrates the robustness of the synthesized materials and their suitability for practical applications in water-splitting technologies. In conclusion, this work underscores the feasibility and advantages of using a solventless synthesis method for designing efficient OER catalysts. The systematic investigation of their electrochemical properties highlights key relationships between composition, structure, and activity, providing valuable insights into the development of advanced catalysts for renewable energy treatments. Future research can build upon these findings by exploring additional compositions, doping strategies, or hybrid systems to further enhance OER performance and scalability. This study

contributes to the ongoing efforts to advance sustainable energy solutions through innovative catalyst design.

References

1. Kalt, G., et al., *Conceptualizing energy services: A review of energy and well-being along the Energy Service Cascade*. Energy Research & Social Science, 2019. **53**: p. 47-58.
2. Vahidi, A. and A. Sciarretta, *Energy saving potentials of connected and automated vehicles*. Transportation Research Part C: Emerging Technologies, 2018. **95**: p. 822-843.
3. Farghali, M., et al., *Integration of biogas systems into a carbon zero and hydrogen economy: a review*. Environmental chemistry letters, 2022. **20**(5): p. 2853-2927.
4. Wang, B., et al., *Technological-economic assessment and optimization of hydrogen-based transportation systems in China: a life cycle perspective*. International Journal of Hydrogen Energy, 2023. **48**(33): p. 12155-12167.
5. Guan, Y., et al., *Burden of the global energy price crisis on households*. Nature Energy, 2023. **8**(3): p. 304-316.
6. Farghali, M., et al., *Strategies to save energy in the context of the energy crisis: a review*. Environmental Chemistry Letters, 2023. **21**(4): p. 2003-2039.
7. Lee, R., *The outlook for population growth*. Science, 2011. **333**(6042): p. 569-573.
8. Christopher, K. and R. Dimitrios, *A review on exergy comparison of hydrogen production methods from renewable energy sources*. Energy & Environmental Science, 2012. **5**(5): p. 6640-6651.
9. Acar, C. and I. Dincer, *Comparative assessment of hydrogen production methods from renewable and non-renewable sources*. International Journal of Hydrogen Energy, 2014. **39**(1): p. 1-12.
10. Azwar, M., M. Hussain, and A. Abdul-Wahab, *Development of biohydrogen production by photobiological, fermentation and electrochemical processes: a review*. Renewable and Sustainable Energy Reviews, 2014. **31**: p. 158-173.
11. Kudo, A., *Photocatalysis and solar hydrogen production*. Pure and Applied Chemistry, 2007. **79**(11): p. 1917-1927.
12. Zheng, Y., et al., *Graphitic carbon nitride polymers toward sustainable photoredox catalysis*. Angewandte Chemie International Edition, 2015. **54**(44): p. 12868-12884.

13. Kong, M., et al., *Tuning the relative concentration ratio of bulk defects to surface defects in TiO₂ nanocrystals leads to high photocatalytic efficiency*. Journal of the American Chemical Society, 2011. **133**(41): p. 16414-16417.
14. Yang, J., et al., *Roles of cocatalysts in photocatalysis and photoelectrocatalysis*. Accounts of chemical research, 2013. **46**(8): p. 1900-1909.
15. Kudo, A. and Y. Miseki, *Heterogeneous photocatalyst materials for water splitting*. Chemical Society Reviews, 2009. **38**(1): p. 253-278.
16. Kalamaras, C.M. and A.M. Efsthathiou. *Hydrogen production technologies: current state and future developments*. in *Conference papers in science*. 2013. Wiley Online Library.
17. Reier, T., M. Oezaslan, and P. Strasser, *Electrocatalytic oxygen evolution reaction (OER) on Ru, Ir, and Pt catalysts: a comparative study of nanoparticles and bulk materials*. Acs Catalysis, 2012. **2**(8): p. 1765-1772.
18. Tee, S.Y., et al., *Amorphous ruthenium nanoparticles for enhanced electrochemical water splitting*. Nanotechnology, 2015. **26**(41): p. 415401.
19. Lee, Y., et al., *Synthesis and activities of rutile IrO₂ and RuO₂ nanoparticles for oxygen evolution in acid and alkaline solutions*. The journal of physical chemistry letters, 2012. **3**(3): p. 399-404.
20. Rossmeisl, J., et al., *Electrolysis of water on oxide surfaces*. Journal of Electroanalytical Chemistry, 2007. **607**(1-2): p. 83-89.
21. Song, J., et al., *A review on fundamentals for designing oxygen evolution electrocatalysts*. Chemical Society Reviews, 2020. **49**(7): p. 2196-2214.
22. Grimaud, A., et al., *Activating lattice oxygen redox reactions in metal oxides to catalyse oxygen evolution*. Nature chemistry, 2017. **9**(5): p. 457-465.
23. Huang, Z.-F., et al., *Chemical and structural origin of lattice oxygen oxidation in Co-Zn oxyhydroxide oxygen evolution electrocatalysts*. Nature Energy, 2019. **4**(4): p. 329-338.
24. Lehmann, H., X. Fuentes-Arderiu, and L. Bertello, *Glossary of terms in quantities and units in Clinical Chemistry (IUPAC-IFCC Recommendations 1996)*. Pure and Applied Chemistry, 1996. **68**(4): p. 957-1000.
25. Nørskov, J.K., et al., *Trends in the exchange current for hydrogen evolution*. Journal of The Electrochemical Society, 2005. **152**(3): p. J23.

26. Xu, K., et al., *Regulating water-reduction kinetics in cobalt phosphide for enhancing HER catalytic activity in alkaline solution*. *Advanced Materials*, 2017. **29**(28): p. 1606980.
27. Ghuman, K.K., S. Yadav, and C.V. Singh, *Adsorption and dissociation of H₂O on monolayered MoS₂ edges: Energetics and mechanism from ab initio simulations*. *The Journal of Physical Chemistry C*, 2015. **119**(12): p. 6518-6529.
28. Fourmond, V., et al., *H₂ Evolution and Molecular Electrocatalysts: Determination of Overpotentials and Effect of Homoconjugation*. *Inorganic Chemistry*, 2010. **49**(22): p. 10338-10347.
29. Shinagawa, T., A.T. Garcia-Esparza, and K. Takanebe, *Insight on Tafel slopes from a microkinetic analysis of aqueous electrocatalysis for energy conversion*. *Scientific reports*, 2015. **5**(1): p. 13801.
30. Thomas, J.M. and W.J. Thomas, *Principles and practice of heterogeneous catalysis*. 2014: John Wiley & Sons.
31. Cai, Z.x., et al., *Electrodeposition-Assisted Synthesis of Ni₂P Nanosheets on 3D Graphene/Ni Foam Electrode and Its Performance for Electrocatalytic Hydrogen Production*. *ChemElectroChem*, 2015. **2**(11): p. 1665-1671.
32. Wei, C., et al., *Approaches for measuring the surface areas of metal oxide electrocatalysts for determining their intrinsic electrocatalytic activity*. *Chemical Society Reviews*, 2019. **48**(9): p. 2518-2534.
33. Carmo, M., et al., *A comprehensive review on PEM water electrolysis*. *International journal of hydrogen energy*, 2013. **38**(12): p. 4901-4934.
34. Can, M.M., T. Karaman, and S. Shawuti, *Optical and structural modification of boron-doped CoGa₂O₄ particles*. *Ceramics International*, 2020. **46**(9): p. 13025-13032.
35. Zhou, S.X., et al., *Synthesis of NiGa₂O₄ octahedron nanocrystal with exposed {111} facets and enhanced efficiency of photocatalytic water splitting*. *ChemPlusChem*, 2015. **80**(1): p. 223-230.
36. Peng, X., et al., *Strategies to improve cobalt-based electrocatalysts for electrochemical water splitting*. *Journal of Catalysis*, 2021. **398**: p. 54-66.

37. Zhang, Q., et al., *Hollow waxberry-like cobalt–nickel oxide/S, N-codoped carbon nanospheres as a trifunctional electrocatalyst for OER, ORR, and HER*. RSC advances, 2020. **10**(46): p. 27788-27793.
38. Wu, J., et al., *Novel nickel–cobalt phosphite with face-sharing octahedra derived electrocatalyst for efficient water splitting*. Inorganic Chemistry Frontiers, 2019. **6**(8): p. 2014-2023.
39. Duraivel, M., et al., *Hierarchical 3D flower like cobalt hydroxide as an efficient bifunctional electrocatalyst for water splitting*. Electrochimica Acta, 2022. **411**: p. 140071.
40. Peng, Z., et al., *From water oxidation to reduction: homologous Ni–Co based nanowires as complementary water splitting electrocatalysts*. Advanced Energy Materials, 2015. **5**(9): p. 1402031.
41. Xu, Z., et al., *Adjusting the crystallinity of mesoporous spinel CoGa₂O₄ for efficient water oxidation*. ACS Applied Materials & Interfaces, 2016. **8**(20): p. 12887-12893.
42. Xue, H., et al., *Hollow Rods of Nanocrystalline NiGa₂O₄: Hydrothermal Synthesis, Formation Mechanism, and Application in Photocatalysis*. Crystal Growth & Design, 2008. **8**(12): p. 4511-4516.
43. Lv, X.-J., et al., *Photocatalytic overall water splitting promoted by SnO_x–NiGa₂O₄ photocatalysts*. Applied Catalysis B: Environmental, 2016. **182**: p. 220-228.
44. Di Quarto, F., et al., *Modeling of Optical Band-Gap Values of Mixed Oxides Having Spinel Structure AB₂O₄ (A = Mg, Zn and B = Al, Ga) by a Semiempirical Approach*. ACS Organic & Inorganic Au, 2024. **4**(1): p. 120-134.
45. Abdullah, M.I., et al., *Ultrasonically Surface-Activated Nickel Foam as a Highly Efficient Monolith Electrode for the Catalytic Oxidation of Methanol to Formate*. ACS Applied Materials & Interfaces, 2021. **13**(26): p. 30603-30613.
46. Vidal-Iglesias, F.J., et al., *Understanding the Nernst Equation and Other Electrochemical Concepts: An Easy Experimental Approach for Students*. Journal of Chemical Education, 2012. **89**(7): p. 936-939.
47. Archer, M.D., *Genesis of the Nernst Equation*, in *Electrochemistry, Past and Present*. 1989, American Chemical Society. p. 115-126.

48. McHugh, P.J., A.D. Stergiou, and M.D. Symes, *Decoupled Electrochemical Water Splitting: From Fundamentals to Applications*. *Advanced Energy Materials*, 2020. **10**(44): p. 2002453.
49. Wang, J., et al., *Recent Progress in Cobalt-Based Heterogeneous Catalysts for Electrochemical Water Splitting*. *Advanced Materials*, 2016. **28**(2): p. 215-230.
50. van der Heijden, O., et al., *Tafel Slope Plot as a Tool to Analyze Electrocatalytic Reactions*. *ACS Energy Letters*, 2024. **9**(4): p. 1871-1879.